AMERICAN UNIVERSITY OF BEIRUT

A NUMERICAL STUDY USING THREE DIFFERENT APPROACHES FOR ENHANCING THE PERFORMANCE OF PV PANELS WITH PHASE CHANGE MATERIALS

by
AMIN ALI WAHAB

A thesis
submitted in partial fulfillment of the requirements
for the degree of Master of Engineering
to the Department of Mechanical Engineering
of the Faculty of Engineering and Architecture
at the American University of Beirut

Beirut, Lebanon
April 2017

AMERICAN UNIVERSITY OF BEIRUT

A NUMERICAL STUDY USING THREE DIFFERENT
APPROACHES FOR ENHANCING THE PERFORMANCE OF
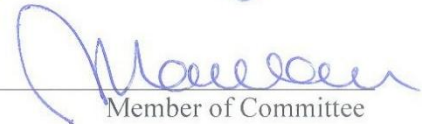PV PANELS WITH PHASE CHANGE MATERIALS

by
AMIN ALI WAHAB

Approved by:

_____

Dr. Fadl Moukalled, Professor   Advisor
Mechanical Engineering

_____

Dr. Marwan Darwish, Professor   Member of Committee
Mechanical Engineering

_____

Dr. Kamel Ghali, Professor   Member of Committee
Mechanical Engineering

April 26, 2017

AMERICAN UNIVERSITY OF BEIRUT

THESIS, DISSERTATION, PROJECT RELEASE FORM

Student Name: _Wahab_ _Amin_ _Ali_
                           Last   First   Middle

☒ Master's Thesis   ◯ Master's Project   ◯ Doctoral
Dissertation

☐   I authorize the American University of Beirut to: (a) reproduce hard or electronic copies of my thesis, dissertation, or project; (b) include such copies in the archives and digital repositories of the University; and (c) make freely available such copies to third parties for research or educational purposes.

☒   I authorize the American University of Beirut, to: (a) reproduce hard or electronic copies of it; (b) include such copies in the archives and digital repositories of the University; and (c) make freely available such copies to third parties for research or educational purposes

after : **One ----**   **year from the date of submission of my thesis, dissertation, or project.**
         Two ----   **years from the date of submission of my thesis, dissertation, or project.**
         (**Three**)**---- years from the date of submission of my thesis, dissertation, or project.**

_____   May 08, 2017

Signature   Date

ACKNOWLEDGMENTS

AN ABSTRACT OF THE THESIS OF

Amin Ali Wahab   for   Master of Engineering
                            Major: Applied Energy

Title: A Numerical Study Using Three Different Approaches for Enhancing the Performance of PV Panels with Phase Change Materials

Enhancing the efficiency of renewable energy technologies has been the focus of numerous research projects in the last decades. One such area of interest has been improving the efficiency of photovoltaic (PV) panels. While PV panels use the most abundant and sustainable energy sources in the planet, they have quite a low efficiency in terms of energy conversion. Partly this low efficiency is due to the increase in surface temperature that occurs during the operation of PV panels. A small number of proven techniques have been developed to decrease the surface temperature. These techniques fall into two groups denoted by active cooling techniques and passive cooling techniques, respectively. Active cooling methods include forced ventilation or hydraulic cooling that requires maintenance and additional costs. On the other hand, the passive cooling methods include natural ventilation, and phase change (PCM) materials. This latter technique has shown promises in harnessing the nocturnal cooling effect with its inherent latent energy storage capacity. The aim of this project is to develop and compare several rigorous numerical approaches for the application of PCM to the passive cooling of PV panels. To this end, models of PV and PV/PCM modules subjected to indoor and outdoor conditions were developed using an in-house code developed within the "MATLAB" environment, the commercial "FLUENT" Computational Fluid Dynamics (CFD) package, and the open source "OpenFOAM" CFD framework. The validation of these models was done by comparison with experimental data obtained from the literature. While the 3-D models simulated in "FLUENT" and "OpenFOAM" exhibited a close match to the experimental data, the 1-D models run in "MATLAB" showed relatively greater discrepancy. A parametric study is also conducted on the validated 3-D models to investigate the effect of varying the radiation load and the PCM type on the performance of the PV and PV/PCM modules.

CONTENTS

ILLUSTRATIONS

TABLES

CHAPTER I

INTRODUCTION

Under ordinary insolation, commercial photovoltaic cell can only convert 10 – 22 % of the solar radiation it receives into electricity depending on the type of the PV cell (Twidell and Weir, 2006). The predicted efficiency of a PV cell at standard test condition (STC) or at standard operating condition is usually higher than its actual efficiency which is greatly affected by reflection losses and solar cell temperature. While STC takes place at 1000 W/m^2 irradiance and 25 ℃ cell temperature, the normal operating cell temperature (NOCT) rating is done under 800 W/m^2 irradiance and at fixed air temperature of 20 ℃. For crystalline silicon solar cells, a reduction in voltage and efficiency can be noticed up to 0.4-0.5% per degree increase in cell temperature (Krauter and Hanitsch, 1996). Radziemska and Klugmann (2002) studied experimentally the performance of a PV module as its temperature increases from 22 ℃ to 70 ℃. Measurements demonstrated deterioration in performance with a reduction in efficiency of 0.65% for every degree increase in temperature. To avoid excessive heating of the PV cell and to attain an operating efficiency of the PV module close to that at STC, many active and passive cooling methods have been developed. The most popular active cooling methods include forced ventilation, heat pipe, and hydraulic cooling; however, regular maintenance and extra power consumption is required for such methods. Passive cooling techniques such as natural ventilation and phase change material are also widely used; nonetheless, natural ventilation using an air duct behind the PV module suffers low heat transfer rates due to the low heat capacity of air and

its dependence on wind; also, the accumulating dust in the duct leads to further reduction in the overall heat transfer (Huang, Eames, and Norton, 2004). In applications with small temperature variations, a latent heat storage system (LHTS) is more reliable than a sensible heat storage system since it has a nearly isothermal and high storage capacity (Lamberg and Sire´n, 2003); the LHTS materials such as phase change materials (PCM) can store 5-14 times more heat per unit volume than sensible heat storage system materials such as rock and masonry (Sharma, Tyagi, Chen, and Buddhi, 2009). PCMs can absorb or discharge large amount of energy in the form of latent heat at a constant phase transition temperature; hence, they are used as a tool for temperature control and passive heat storage in many applications such as electronics, gypsum wall boards, building roofs, and PV panels (Huang et al., 2004). While heat is absorbed by the PCM during its phase change from solid to liquid, heat is released from the PCM upon undergoing the reverse change in phase from liquid to solid. When overheating occurs in a PV module and the operating efficiency drops down, using PCM material can be very convenient to absorb excessive heat that would be later discharged to the surrounding air during night when no electric power is extracted from the module.

PCM materials can be classified into three main categories classified as organic, inorganic, and eutectic; many of these materials can be found in any required temperature range. In general, the volumetric latent heat storage capacity in inorganic compounds is almost twice that in organic compounds. Organic materials are categorized into paraffin and non-paraffin materials. Paraffin wax is constituted mainly from a straight chain n-alkanes [CH3–(CH2)–CH3] mixture. In addition, paraffin is characterized by its reliability, predictability, safety, low cost, and non-corrosiveness; it has also a low pressure in the melt

form; thus, a system employing paraffin would have a long melt-freeze cycle. On the other hand, the largest number of PCMs is of the non-paraffin organic materials type. These materials have great diversity such that each one of them has its own features; in contrast, all paraffin organic materials share very similar characteristics. The main subcategory of the non-paraffin materials is fatty acids; they are generally characterized by inflammability, low thermal conductivity, varying level of toxicity, high heat of fusion, low flush points, and instability at high temperatures. Moreover, inorganic compounds are divided into two main categories salt hydrate and metallic. Salt hydrates can be considered as an alloy of inorganic salts and water that composes a typical crystalline solid. The dehydration or hydration of the salt represents the freezing or melting of the salt hydrate material. The usage of salt hydrates in latent heat thermal energy storage systems has been extensively investigated as they are considered the most significant class among PCMs. Salt hydrates are characterized by their relatively high thermal conductivity which is nearly twice that in paraffin.
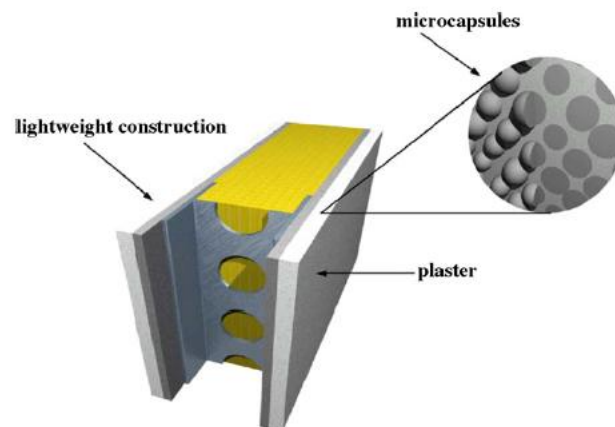
Figure 1.1: Schematic view of a lightweight wall. The PCM micro-capsules are integrated into the interior plaster (Sharma et al., 2009)
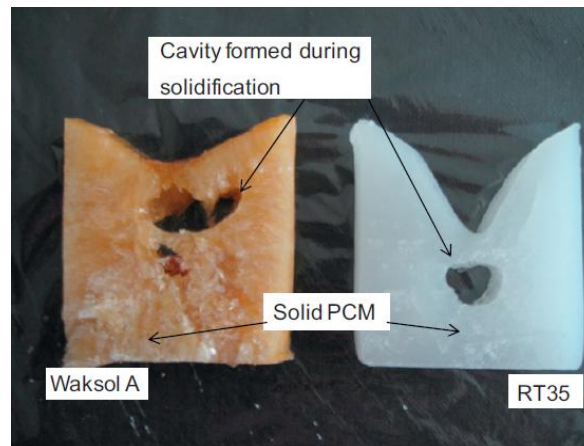
Figure 1.2 The porosity formed in the central bulk of PCM Waksol A and RT35 during solidification (Huang, Eames, Norton, and Hewitt, 2011)

Also, they have high latent heat of fusion per unit volume, small volume changes upon melting, low corrosiveness, low cost, and low toxicity. The other class of inorganic PCMs is metallic. While the heavy weight of this material prevented its usage in PV applications, metallic has high thermal conductivity, low heat of fusion per unit weight, and high heat of fusion per unit volume. Finally, the third main category of PCMs is eutectics. In this class, a composition is made up of two or more components where all the components freeze and melt congruently such that a mixture of component crystals is formed during crystallization. In addition, eutectics are distinguished by their minimum melting point; for instance, the melting point of hexadecane-tetradecane mixture is as low as 1.7 ℃ (Sharma et al., 2009).
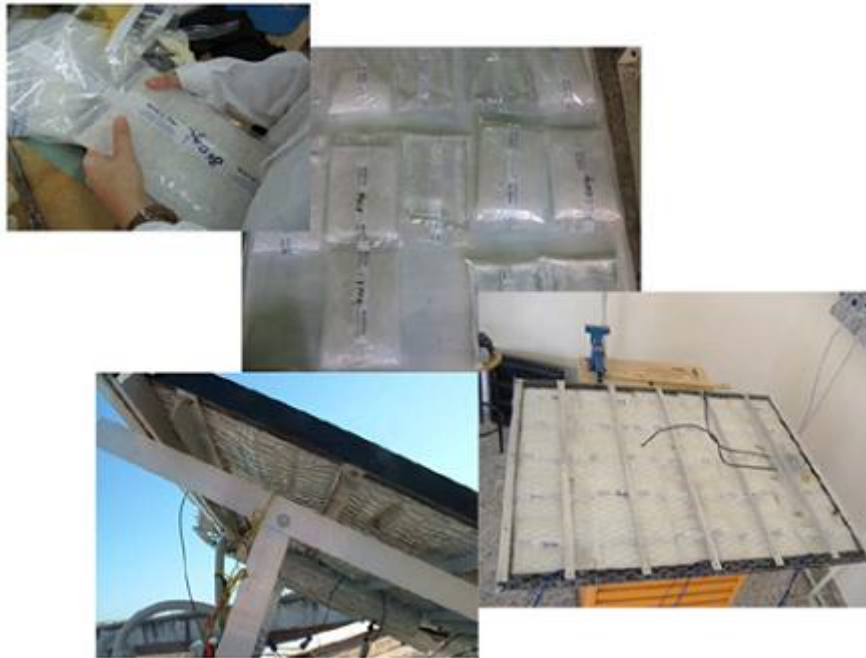
Figure 1.3: The encapsulated PCM and its installation (Lo Brano, Ciulla, Piacentino, & Cardona, 2013).

A. LITERATURE REVIEW

Huang, Eames, and Norton (2006a) evaluated experimentally the thermal regulation capacity of PCM in a photovoltaic system. Experiments were conducted on three different PV/PCM systems with distant fins arrangement using two types of commercial PCMs the RT25 and GR40; the system having 32 fins and using RT25 was capable of maintaining the temperature of the front surface at 29 ℃ for about two hours under $750\ W/m^2$ insolation and 23 ℃ ambient temperature. Also, GR40 proved to be less effective than RT25 in terms of decreasing PV surface temperature. Huang et al. (2011b) investigated experimentally the effect of using PCM on the temperature control of the front surface of a building integrated photovoltaic device for different fins spacing configurations in the PV/PCM system. Higher

fin spacing reduced convection and thermal stratification inside the PV/PCM system and allowed a longer time for the complete melting of the PCM. Further, Hasan, McCormack, Huang, and Norton (2010) conducted a series of experiments on five types of PCMs where each of them was placed in four different PV/PCM system at three different insolation. The impacts of the thermal conductivities of the PCM, the PV/PCM system configuration, and the thermal mass of the PCM were evident on the thermal regulation yield of the PCM. At lower PV operating temperature better results were achieved with the PCM with lower thermal conductivity and melting point (capric-palmitic acid C-P) while the PCM with higher thermal conductivity and melting point (pure salt hydrate $CaCl_2$) performed better at higher PV operating temperature. Among the different PCM types, $CaCl_2$ reduced the PV front surface temperature by 10℃ for five continuous hours at 1000 W/m^2. The first numerical model simulating the cooling effect of PCM in a PV system that has been validated experimentally was developed by Haung et al. (2004). It has been shown that the PV/PCM system of type 3 (with 2 fins) can maintain a PV surface temperature of 36.4 ℃ for 80 minutes under 1000 W/m^2 insolation and 20 ℃ ambient temperature. This numerical model was later developed by Huang et al. (2006b) to become three dimensional; a good agreement was found in the predictions between the two models. Moreover, two different numerical algorithms based on enthalpy method and effective heat capacity method were applied using "FEMLAB" software by Lamberg, Lehtiniemi, and Henell (2004) to investigate the usage of PCM as a means to balance temperature variations in electronics and buildings. In their study, an experimental PCM storage apparatus was constructed for the sake of validating the numerical results generated by FEMLAB.
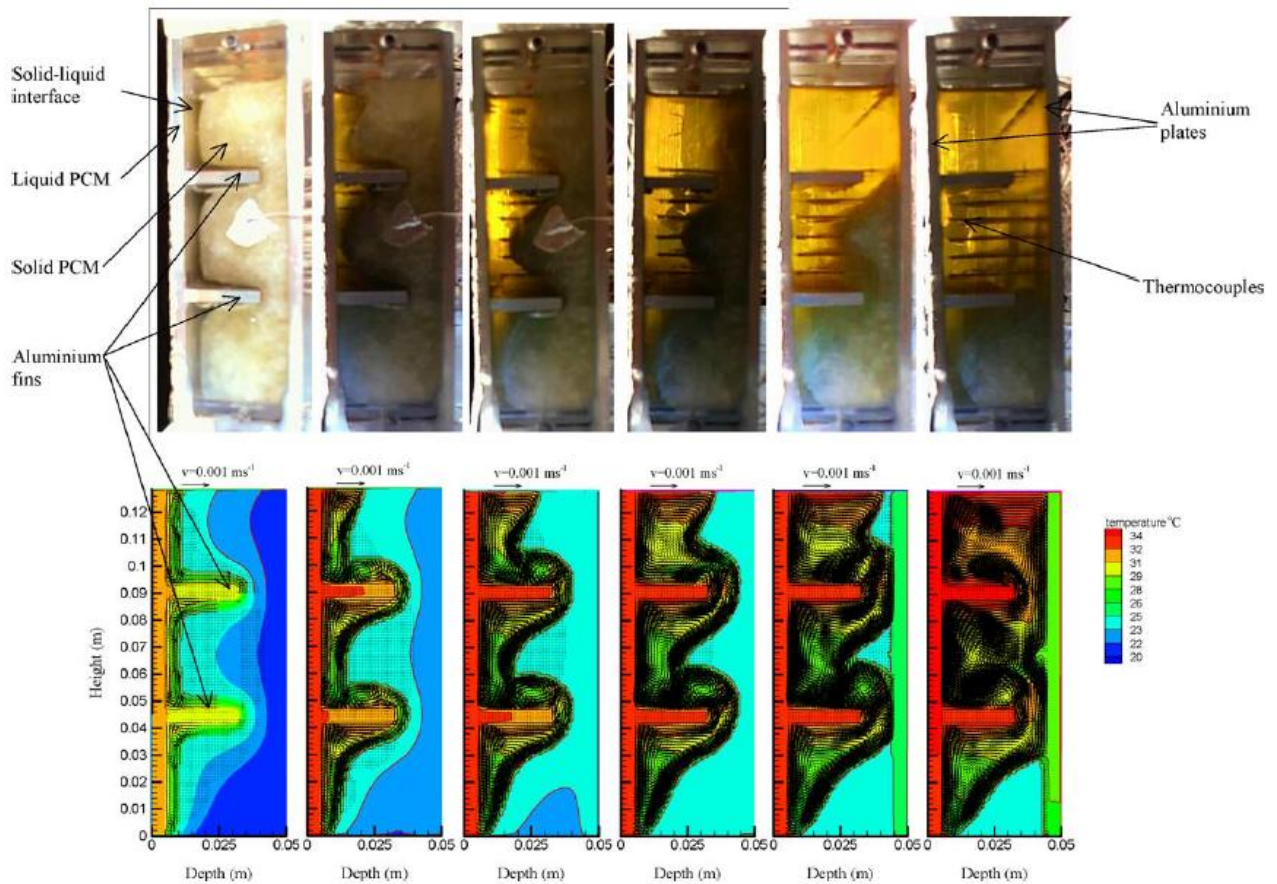
Figure 1.4: Photovoltaic image and predicted isotherms and velocities for a PV/PCM system with fins during the PCM melt process (Huang et al., 2004).

The experimental results compared well with numerical predictions; however, the effective heat capacity method proved to be more accurate for narrower phase change temperature range of 2 ℃. Besides, integrating multiple combinations of pairs of PCM materials that have different phase transient temperatures in a PV/PCM system have been investigated numerically by Huang (2011a) in terms of heat regulation improvement. Comparing the results of the different PCM combinations showed that the RT27-RT21 pair yields the highest decrease in temperature. Malvi, Dixon-Hardy, and Crook (2011) simulated a

combined photovoltaic solar-thermal system that contains layers of phase change material. A parametric study investigating the effects of varying the flow rate, water temperature, PCM thickness and its melting point was performed. The study demonstrated that enhancement in performance of the PV module occurs at the expense of the performance of the solar-thermal system; also, such a combined system can achieve a 9 % higher PV output compared to a conventional PV system. Ho et al. (2012) conducted numerical simulations of a microencapsulated phase change material layer integrated in a photovoltaic device to predict its thermal and electric performance; upon using a PCM layer with a melting temperature of 26℃ and aspect ratio 0.277, the minimum efficiency of the module was improved by 0.13 % and 0.42 % for summer and winter seasons respectively. Hendricks and van Sark (2013) modeled the annual energy output of a PV/PCM system using a simplified heat balance. Estimates of the energy output gain resulting from this system at two different locations and using different PCM types were calculated numerically; also, a cost analysis including the payback period was performed for the different cases considered. Biwole, Eclache, and Kuznik (2013) proposed a mathematical model for the heat and mass transfer of a module made up of PCM RT25 that is placed at the back of a solar panel; the model was solved numerically using finite element method where the solar panel was represented by an aluminum plate. Then, two experiments were carried out using particle image velocimetry (PIV) to validate the results obtained from the numerical model for both the velocity field and the moving solid-liquid boundary inside the PCM container. The simulated results showed that under 1000 W/m^2 insolation, this device can sustain the panel's temperature under 40 ℃ for 80 minutes. Furthermore, Lo

Brano, Ciulla, Piacentino, and Cardona (2013) proposed a simplified numerical model for a PV/PCM module based on one dimensional geometry. The model was established on two sets of recursive equations that can be implemented for two different types of spatial domains; the phase change was considered strictly isothermal. Data obtained from a test facility was compared with the results acquired from the proposed numerical algorithm; the thermal model proved its reliability under distant climatic conditions as the difference between the calculated and measured silicon temperature did not exceed 5 %. In addition, Park, Kim, and Leigh (2014) assessed the performance of a PV/PCM module under realistic outdoor climatic conditions. The experiments were conducted at Incheon, South Korea in May and June for different PCM thicknesses and yielded a maximum drop in PV temperature of 5 °C compared to the conventional PV module. This experimental data was used to validate a simulation method that computes the module temperature and energy generation using "TRNSYS" software; the predicted PV temperature did not deviate more than 5.4 % from the corresponding experimental results. The validated simulation method was then used to carry out a parametric study on the PV/PCM module regarding the installation direction of the module and the melting temperature of the PCM. Finally, an outdoors examination of a PV/PCM system was conducted experimentally by Hasan et al. (2015) under two different climates at Ireland and Pakistan using two types of PCMs; also, numerical simulations were performed under the same conditions of the experiments and the difference between the two results was not more than 6.3 %. Both PCMs performed better regarding limiting the PV temperature rise at Pakistan where hot and stable climate dominates than in Ireland that is overwhelmed by variant weather.

In this study, the performance of PCM as a passive cooling means for both indoor and outdoor PV modules will be investigated numerically. Experimental data from the literature will be used to validate the developed 1-D and 3-D numerical models of the PV and PV/PCM systems. Also, a parametric study based on the applied radiation load and the thermo-physical properties of the PCM will be carried out on the validated models.

CHAPTER II

GOVERNING EQUATIONS AND DISCRETIZATION

Numerical methods for solving transfer phenomena problems encountered in many engineering applications have evolved over the past few decades. The aim of all these methods is to replace the exact continuous solution of the governing partial differential equations by discrete values at specified locations (Moukalled et al., 2016). One of the most widely used methods is the "Finite Volume Method" adopted here. In this method, solutions are sought at discrete locations denoted by "grid points" with each one residing at the centroid of its surrounding element; the aggregation of these non-overlapping elements constitutes the calculation domain. The values of the dependent variable at the grid points represent the primary unknowns (Patankar, 1980). The governing differential equations are integrated over each cell. Then, the volume integrals of the diffusion and convection terms are transformed into surface integrals using the divergence theorem, known also as Green's theorem (Hackbusch 1985; Hackbusch 1994; Murthy and Mathur 2002); these surface integrals are changed into summation of fluxes over the faces of the elements. Next, integration points are employed to evaluate the discrete integrals resulting from the surface and volume integrals (Moukalled et al., 2016). The fluxes of the different terms are solved using appropriate schemes which are profiles representing the change in the dependent variable between the grid points. As a result, the governing differential equations are transformed into sets of algebraic equations called the "discretization equations"; the

solution of these equations generates the dependent variable distribution fields; discretization equations are written in the following general form:

$$a_p \phi_p = \sum a_{nb} \phi_{nb} + b \qquad (2.1)$$

Where ϕ_p and ϕ_{nb} represent the dependent variable values at the centroid of the main element and the centroids of the neighboring elements, respectively, while a_p and a_{nb} are their respective coefficients. The conservation principle of a physical quantity ϕ such as mass, momentum, and energy which is inherent in the governing differential equations of an infinitesimal element is conveyed to the discretization equations of a finite element; this integral conservation of the different physical quantities holds over any group of elements regardless of mesh refinement. As the number of elements considered increases, the distances between grid points decrease; hence, the change of ϕ among neighboring grid points is reduced and the details of the assumed profiles become minor. Consequently, the approximate solution of the discretization equations gets closer to the exact solution of the differential equations (Patankar, 1980).

In a collocated grid, all variables are stored at the centroids of the elements; however, it carries the risk of producing a checkerboard pressure and velocity fields that would be sensed by the numerical scheme as uniform fields. The staggered grid formulation was suggested to solve this problem via enforcing the coupling between the velocity and pressure fields. This coupling is attained by staggering the storing locations of the different variables such that all variables including pressure are stored at the cell centroid except for the velocity field, it is stored at the cell faces. Hence, the calculation of the velocity field and pressure gradient in the continuity and momentum equations

respectively require no interpolation. Nevertheless, complications arise in this grid formulation method since in two and three dimensional problems, three and four staggered grid systems will be required respectively to integrate the velocity components over the elements; also, the complexity increases for Cartesian and unstructured grids such that all Cartesian velocity components would have to be staggered in all directions to ensure that all the faces have all velocity components which leads to doubling the number of momentum equations that are required to be solved in two dimensional problems. After developing the innovative Rhie-Chow interpolation which computes a momentum satisfying mass flow rate field at the element faces, the deficiency presented earlier in the cell centered collocated grid system was solved and this system became once again a more convenient system to be used for obtaining a numerical solution. As a result, the SIMPLE algorithm was developed for the collocated grid. The pressure correction equation was obtained by substituting the correction fields of the discrete momentum equation into the expanded form of the continuity equation so that mass conservation is enforced (Moukalled et al., 2016).

The SIMPLE (Semi Implicit Method for Pressure Linked Equations) algorithm that was developed by Patankar and Spalding solves iteratively the flow problems by obtaining pressure and velocity fields which sequentially satisfy the momentum and continuity equations. To attain a solution for a single time step, the SIMPLE algorithm starts with the initial guesses $P^{(n)}$, $u^{(n)}$, and $\dot{m}^{(n)}$ for the fields of pressure, velocity, and mass flow rate respectively. Next, the momentum equation is solved to generate a new velocity field u^*. The latter field of velocity is used to calculate a momentum satisfying mass flow rate field

$\dot{m}^*$ via Rhie-Chow interpolation. After substituting the new mass flow rate value in the

pressure correction equation, the pressure correction field $\acute{P}$ is obtained. Furthermore, the

velocity, mass flow rate, and pressure fields are updated using $\acute{P}$ field to obtain,

respectively, the u^{**}, $\dot{m}^{**}$, and P^* fields that satisfy the continuity equation. Finally, the

latter values of the velocity, mass flow rate, and pressure fields are considered as initial

guesses for the next iteration; the momentum equation is solved again and all the following

steps are repeated until achieving a converged solution. In general, the solution methods for

the generated algebraic system of equations can be grouped into two categories direct and

iterative. The same solution should be attained for the same set of discrete equations

regardless of the solution method employed which is independent of the discretization

method (Moukalled et al., 2016).

In this study, the Finite Volume Method (FVM) was employed to obtain the

temperature distribution of the model's front surface for the various PV and PV/PCM

modules considered and across all the software frameworks involved. The equations

governing the different models of the PV and PV/PCM modules are listed below.

$$\frac{\partial}{\partial t}(\rho) + \nabla.(\rho\boldsymbol{v}) = 0 \tag{2.2}$$

$$\frac{\partial}{\partial t}(\rho\boldsymbol{v}) + \nabla.(\rho\boldsymbol{v}\boldsymbol{v}) = \nabla.\tau - \nabla p + \rho\boldsymbol{g} \tag{1.3}$$

$$\frac{\partial}{\partial t}(\rho H) + \nabla.(\rho\boldsymbol{v}H) = \nabla.(K\nabla T) \tag{2.4}$$

$$H = h + \Delta H \tag{2.5}$$

$$h = h_{ref} + \int_{T_{ref}}^{T} c_p dT \cong c_p T \tag{2.6}$$

$$\frac{\partial}{\partial t}(\rho h) + \nabla.(\rho \boldsymbol{v} h) = \nabla.(K\nabla T) - \left(\frac{\partial}{\partial t}(\rho \Delta H) + \nabla.(\rho \boldsymbol{v} \Delta H)\right) \qquad (2.7)$$

$$\frac{\partial}{\partial t}(\rho h) = \nabla.(K\nabla T) - \frac{\partial}{\partial t}(\rho \Delta H) \qquad (2.8)$$

$$\frac{\partial}{\partial t}(\rho c_p T) = \nabla.(K\nabla T) - \frac{\partial}{\partial t}(\rho \Delta H) \qquad (2.9)$$

$$\Delta H = \alpha L \qquad (2.10)$$

For the phase change material region, the Enthalpy method is commonly used to solve diffusion phase change problems. Fixed grid solutions can be obtained because conditions on temperature, velocity, and heat removal that are required at the phase change front will not be needed when the enthalpy approach is used (Voller et al., 1987; ANSYS 2011). Equation 2.7 was derived from Equation 2.4 which represents the energy conservation equation in its total enthalpy form. Equation 2.5 and Equation 2.6 are the equations of the total and sensible enthalpy respectively. Equation 2.7 which represents the energy conservation equation in its enthalpy form resulted from substituting Equation 2.5 into Equation 2.4. Equation 2.7 was reduced into Equation 2.8 by neglecting the convective heat transfer terms because the PCM material experiences weak natural convective currents. After substituting Equation 2.6 into Equation 2.8, Equation 2.9 was obtained which represents the energy conservation equation in its reduced temperature form. As the enthalpy-porosity method will be used to model the melting/solidification process, Equation 2.10 represents the relation between the latent enthalpy ΔH and the PCM latent energy L through the liquid mass fraction α which varies between 0 and 1. In the Phase change material region, only the conservation of mass equation (Equation 2.2) was applied

beside the energy conservation equation either in its enthalpy form (Equation 2.7) or reduced temperature form (Equation 2.9) depending on the software used; whereas, the equation of conservation of momentum (Equation 2.3) was neglected because weak natural convective currents exist in the PCM material which is usually confined in microcapsules. In the outdoor air region, Equation 2.2, Equation 2.3, and Equation 2.7 were used which represent the conservation equations of mass, momentum, and energy (enthalpy form) respectively. For the air region, the latent enthalpy ΔH is set to zero. In other regions such as PV cell, glass, Perspex, and aluminum, only the equations of conservation of mass and energy (enthalpy, reduced enthalpy, or temperature forms depending on the software used) were considered; thus, only Equation 2.2 and Equation 2.7/2.8/2.9 were solved.

For all 1-D models that were solved in MATLAB, the energy conservation equation was used in its reduced temperature form (Equation 2.9) while the enthalpy form (Equation 2.7) was used for all the 3-D models simulated in FLUENT. On the other hand, the enthalpy form (Equation 2.7) and reduced enthalpy form (Equation 2.8) of the energy conservation equation were respectively used for the fluid and solid regions in all the 3-D models simulated in OpenFOAM.

CHAPTER III

SOFTWARE

The literature survey reported in a previous chapter indicated that most of the PV/PCM modules investigated experimentally or numerically were set indoors under controlled conditions; whereas, few experiments and simulations were conducted outdoors under actual weather conditions. In this study, the performance of PV and PV/PCM modules subjected to indoor and outdoor conditions was assessed using an in-house code developed within the "MATLAB" environment, the commercial "FLUENT" Computational Fluid Dynamics (CFD) package, and the open source "OpenFOAM" CFD framework. The validation of these simulations was achieved using experimental data from Hasan et al. (2010) and Park et al. (2014) for indoor and outdoor simulations respectively.

A. MATLAB

The commercial software "MATLAB" was used to create four 1-D models for numerically studying the performance of PV and PV/PCM modules under specified indoor and outdoor conditions. An implicit discretization method is adopted for all models and the resultant sets of algebraic equations were solved using the TDMA.

1. Indoor PV Module

A 1-D model that represents the three-layer PV cell studied experimentally by Hasan et al. (2010) is simulated numerically in "MATLAB" with its governing equation
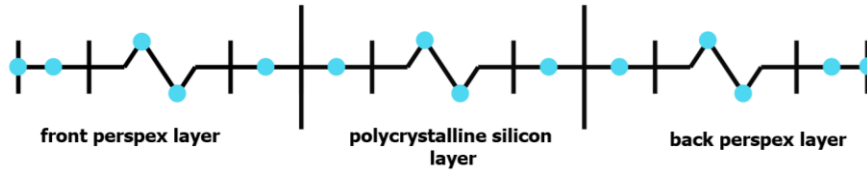
Figure 3.1: Indoor PV module 1-D model

discretized in the context of the Finite Volume Method (FVM). As shown in Figure 3.1, the

three layers composing the model are made of: front perspex, polycrystalline silicon, and

back perspex. The thickness and number of elements, layer thickness, and the number of

nodes (grid points) for each layer are shown in Table 3.1 below.

Table 3.1: Layers properties of the indoor PV module 1-D model

layer name	layer thickness (mm)	number of nodes in the layer	number of elements in the layer	thickness of each element in the layer (mm)
front perspex	3	10	10	0.333
polycrystalline silicon	0.5	4	3	0.167
back perspex	3	10	10	0.333

Thermo-physical properties of perspex and polycrystalline silicon materials that are used in

the model are listed in Table 3.2 shown below.

Table 3.2: Thermo-physical properties of the materials used in the "MATLAB" and "FLUENT" models

	air	Paraffin Wax RT20	Paraffinic Hydrocarbon	Acrylic (pmma)	Aluminum	Glass	Perspex	Polycrystalline Silicon
Density (Kg/m^3)	1.225[c]	825[a]	820[b]	1190[e]	2719[c]	3000[g]	1190[e]	2330[g]
Specific Heat Capacity (J/Kg.K)	1006.43[c]	2100[a]	2100[b]	1470[f]	871[c]	500[g]	1470[f]	677[g]
Thermal Conductivity (W/m.K)	0.0242[c]	0.2[a]	0.2[b]	0.189[e]	237[c]	1[h]	0.189[e]	148[g]
Solidus Temperature (K)	_	294.38[a]	298[b]	_	_	_	_	_
Liquidus Temperature (K)	_	298.88[a]	298[b]	_	_	_	_	_
Latent Heat (J/Kg)	_	140300[a]	184000[b]	_	_	_	_	_
Dynamic Viscosity (Kg/m.s)	1.7894×10^{-5}[c]	0.205[d]	0.205[d]	_	_	_	_	_

Table references: (a- Hasan et al., 2010), (b- Park et al., 2014), (c- "FLUENT" materials

database), (d- Ettouney et al., 2006), (e- Perspex Design Guide – LuciteLux), (f-

www.builditsolar.com), (g- Armstrong et al., 2010), (h- Wilkes et al., 1996).

The external 750 W/m^2 indoor radiation applied in Hasan et al. (2010) experiment

at the front element of the PV module was linearized using the long wave radiation heat

exchange equation to yeild

$$Qr = \varepsilon\sigma(Ts^2 + Text^2)(Ts + Text)(Ts - Text) \qquad (3.1)$$

Where the external emissivity ε and the external radiation source temperature T_{ext} were set

to 0.3869 and 430 K respectively. The ambient air temperature was set at 293.15 K, the

value suggested by Hasan et al. (2010). Since no data was provided by the authors

concerning the type of air convection type around the PV module, forced convection was

assumed with a heat transfer coefficient value of 8 W/m^2K for air at the front and back

sides of the model. The initial temperature was set at 283 K. The model was run for 600

steps using a constant time step with value of 10 s.

2. *Indoor PV/PCM Module*

The second one-dimensional "MATLAB" model simulates the PV/PCM module

composed of six layers, which was studied experimentally by Hasan et al. (2010). As

shown in Figure 3.2, the six layers are front perspex, polycrystalline silicon, and back

perspex, front aluminum, paraffin wax (RT 20), and back aluminum.

front perspex layer   polycrystalline silicon layer   back perspex layer   front aluminum layer   paraffin wax (rt-20) layer   back aluminum layer
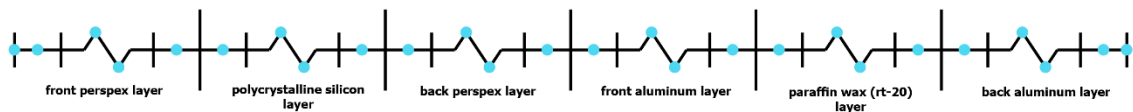
Figure 3.2: Indoor PV/PCM module 1-D model

The thickness and number of elements, layer thickness, and the number of nodes (grid

points) for each layer are shown in Table 3.3 below. The thermo-physical properties of

perspex, polycrystalline silicon, aluminum, and paraffin wax materials that were used in the

model are listed in Table 3.2.

Table 3.3: Layers properties of the indoor PV/PCM module 1-D model

layer name	layer thickness (mm)	number of nodes in the layer	number of elements in the layer	thickness of each element in the layer (mm)
front perspex	3	10	10	0.333
polycrystalline silicon	0.5	4	3	0.167
back perspex	3	10	9	0.333
front aluminum	5	16	15	0.333
paraffin wax (RT 20)	50	150	149	0.336
back aluminum	5	16	16	0.333

The external 750 W/m^2 indoor radiation imposed at the front element of the PV/PCM module is modeled following the same approach described above for the indoor PV module i.e. the external emissivity ε and the external radiation source temperature T_{ext} were set to 0.3869 and 430 K, respectively. In the mushy zone, melting in the paraffin wax layer is modeled according to the equation below:

$$\frac{\partial}{\partial t}(\rho\Delta H) = \frac{\partial}{\partial t}(\rho\beta L) = \rho L\frac{\partial}{\partial t}\left(\frac{Tc-Ts}{Tl-Ts}\right) = \frac{\rho L}{\Delta t}\left(\frac{Tc-Tc^0}{Tl-Ts}\right) \ when \ Ts < Tc < Tl \quad\quad (3.2)$$

where β, L, Tl, Ts, Tc, and Tc^0 are the liquid fraction, heat of fusion, liquidus temperature, solidus temperature, element centroid temperature at the current time step, and element centroid temperature at the previous time step in the paraffin wax layer, respectively. The ambient air temperature was set to 293.15 K. Air was assumed to be naturally convected, as no data was provided by the authors, with a heat transfer coefficient value of 3 W/m^{2}K for air at the front and back sides of the PV/PCM module. While the initial temperature was

kept the same as in the indoor PV module case, the number of time steps was increased to 720 steps each having a fixed size of 30 s.

3. *Outdoor PV Module*

The third 1-D model developed in "MATLAB" simulates an outdoor PV module using the FVM. The model is composed of two layers and replicates numerically the experiment conducted by Park et al. (2014). The two layers of the model are schematically depicted in Figure 3.3 and represent glass and polycrystalline silicon.
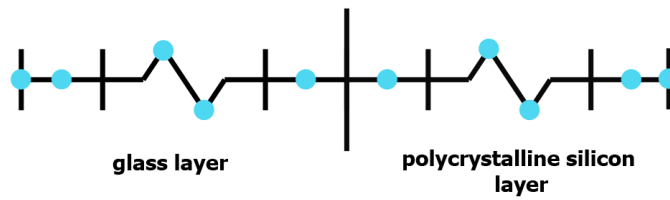
Figure 3.3: Outdoor PV module 1-D model

The thickness and number of elements, layer thickness, and the number of nodes (grid points) for each layer are shown in Table 3.4 below. The thermo-physical properties of glass and polycrystalline silicon materials used in the model are listed in Table 3.2.

Table 3.4: Layers properties of the outdoor PV module 1-D model

layer name	layer thickness (mm)	number of nodes in the layer	number of elements in the layer	thickness of each element in the layer (mm)
glass	2.5	9	9	0.313
polycrystalline silicon	2.5	9	9	0.313

a. Solar Radiation Model

The solar radiation experienced by the PV module is modeled based on "ASHRAE clear sky model" and also using the solar radiation values that were measured via a pyranometer and provided by Park et al. (2014). The pyranometer operates in two modes; (i) if exposed to direct solar radiation, then it measures the total incident radiation on a surface; (ii) if shaded from direct radiation, then it measures the diffuse radiation. According to "ASHRAE clear sky model", the total incident solar radiation on an arbitrary surface is given by the following equation:

$$It = I_D + I_d + I_R \qquad (3.3)$$

$$It = \left[C_N \cos \theta + C \frac{1+\cos \Sigma}{2} + \rho_g \frac{1-\cos \Sigma}{2} (C_N \cos \theta_H + C) \right] I_{DN} \qquad (3.4)$$

$$I_{DN} = \frac{A}{e^{(B/\sin \beta)}} \qquad (3.5)$$

$$\cos \theta_H = \sin \beta \qquad (3.6)$$

$$\cos \theta = \cos \beta \cos \gamma \sin \Sigma + \sin \beta \cos \Sigma \qquad (3.7)$$

$$\sin \beta = \cos l \cos h \cos d + \sin l \sin d \qquad (3.8)$$

$$d = 23.45 \sin \left[\frac{360(284+n)}{365} \right] \qquad (3.9)$$

$$\gamma = |\phi - \psi| \qquad (3.10)$$

$$\cos \phi = (\cos d \sin l \cos h - \sin d \cos l)/\cos \beta \qquad (3.11)$$

$$h = 15(LST - 12) \qquad (3.12)$$

$$LST = LCT + E - DT \qquad (3.13)$$

$$E = 0.165 \sin 2b - 0.126 \cos b - 0.025 \sin b \qquad (3.14)$$

$$b = 360 \left(\frac{n-81}{364} \right) \qquad (3.15)$$

23

$$LCT = CT + \frac{L_{std} - L_{loc}}{15} \qquad (3.16)$$

where I_D, I_d, I_R, and I_{DN} are the direct, diffuse, reflected, and direct normal solar radiation respectively. Moreover, C_N is the atmospheric clearness number, A is the apparent direct normal solar flux at the outer edge of the earth's atmosphere, B is the apparent atmospheric extinction coefficient, C is the ratio of diffuse radiation on a horizontal surface to direct normal radiation, and ρ_g is the ground reflectivity. Furthermore, Σ, θ, θ_H, β, γ, ϕ, and ψ are the surface tilt angle, incidence angle, zenith angle, altitude angle, surface-solar azimuth angle, solar azimuth angle, and surface azimuth angle respectively. These angles can be calculated once the latitude (l), the declination (d), and the hour angle (h) are known. The hour angle is computed from Local solar time (LST), which is related to local civil time (LCT), clock time (CT), the equation of time (E), the daylight saving time (DT), and the day of the year (n). Finally, L_{std} and L_{loc} are the standard meridian for the local time zone and the longitude at the actual location respectively.

The outdoor experiment which was modeled in this study was conducted by Park et al. (2014) at Incheon, South Korea on June 15 2012. The module was placed in a vertical position facing south while measurements of the PV cell temperature were recorded for 24 hours. At this location, the time one is +9 and the corresponding L_{std} is -135°. L_{loc} and l are -126.65° West and 37.38° North respectively. On the day of the experiment, n equals 166. C_N is assumed to be equal to 1. According to "ASHRAE" tables C equals 0.134 in June. Due to the vertical position of the module, the surface tilt angle Σ equals 90°. Ground reflectivity normally equals 0.3. Consequently, total incident solar radiation equation reduces to:

$$It = \left[\cos\theta + \frac{0.134}{2} + \frac{0.3}{2}(\cos\theta_H + 0.134)\right]I_{DN} \qquad (3.17)$$

To obtain more accurate results, I_{DN} was not calculated using the equation from "ASHRAE clear sky model" rather it was calculated using the radiation values measured by the pyranometer. Since it was not stated by Park et al. (2014) whether the pyranometer was operating in the direct or shaded mode, I_{DN} was calculated for both cases. For calculating I_{DN} assuming direct mode of operation of pyranometer, the equation below was used:

$$I_{DN} = It(direct\ mode)/\left[\cos\theta + \frac{0.134}{2} + \frac{0.3}{2}(\cos\theta_H + 0.134)\right] \qquad (3.18)$$

For calculating I_{DN} values based on the assumption that the radiation values were measured by a shaded pyranometer, the equation below was used where the direct component was omitted:

$$I_{DN} = It(shaded\ mode)/\left[\frac{0.134}{2} + \frac{0.3}{2}(\cos\theta_H + 0.134)\right] \qquad (3.19)$$

After comparing the graphs of the two computed sets of I_{DN} values to the distribution of the total radiation It provided by Park et al. (2014), it turned out that the I_{DN} values obtained by assuming a shaded mode of operation of the pyranometer have a similar graphical distribution to that of the measured total radiation. As a result, the values of I_{DN} which were obtained by the latter method were used to calculate the values of I_D, I_d, and I_R components based on "ASHRAE clear sky model" equations stated above at every time step. The resulting values of I_{DN} and I_d that were used in the model are depicted in Figure 3.4.
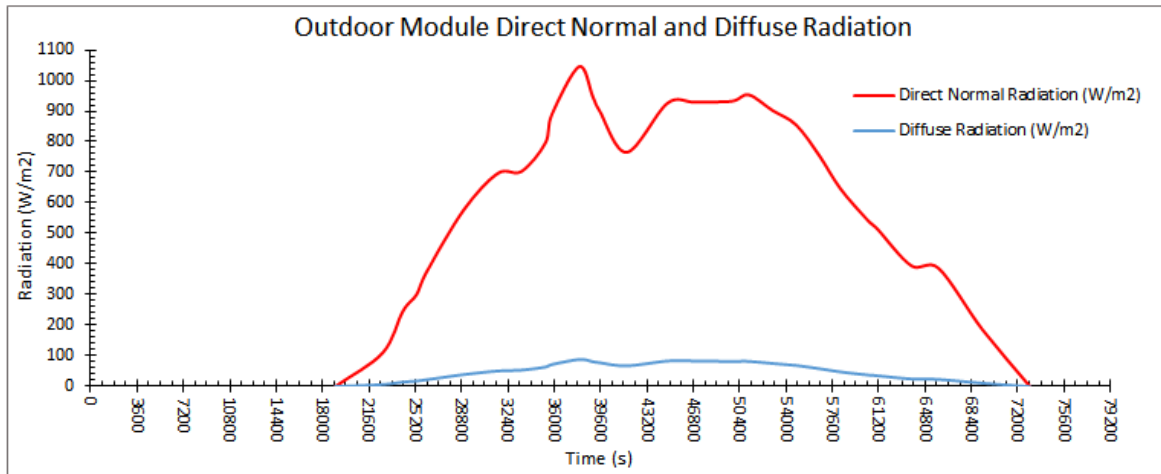
Figure 3.4: Direct normal and diffuse radiation used in modeling outdoor module

b. External Convection Model

The authors did not provide any data concerning the velocity and heat transfer coefficients of air. Using the location and date of the experiment, the direction and magnitude of the velocity were obtained as south-east direction and 13 Km/h (3.61 m/s), respectively, from the historic weather database at "wunderground.com". Based on Ito (1972) model for forced convection transfer, windward surfaces that are exposed to a wind velocity U > 2 m/s, have a surface air velocity u and convection heat transfer coefficient h according to the equations below:

$$u = 0.25U \qquad (3.20)$$

$$h = 3.5 + 5.6u \qquad (3.21)$$

For a wind velocity U of magnitude 3.61 m/s, the resulting value of h is 8.56 w/m.K. The latter calculated value of heat transfer coefficient of air was used at the front and back sides of the model.

c. Absorption and Transmission Models

Since the absorptivity α and transmissivity τ values of the front glass layer used in the experiment were not provided by Park et al. (2014), α and τ were assigned the values of 0.05 and 0.76 respectively based on commercial glass catalogues. While the first element in the glass layer experiences a solar radiation value of αIt, all other subsequent elements are affected by a solar radiation value of $\alpha \tau^{(i-1)} It$ where i is the number of elements. As a result, transmissivity is accounted for when including the effect of solar load in the source term of the algebraic equation for any element throughout the glass layer.

d. Ambient Air Temperature

The air temperature distribution across 24 hours which is shown in Figure 3.5 was also retrieved from the historic weather database at "wunderground.com" using the location and the date when Park et al. (2014) performed their experiment.
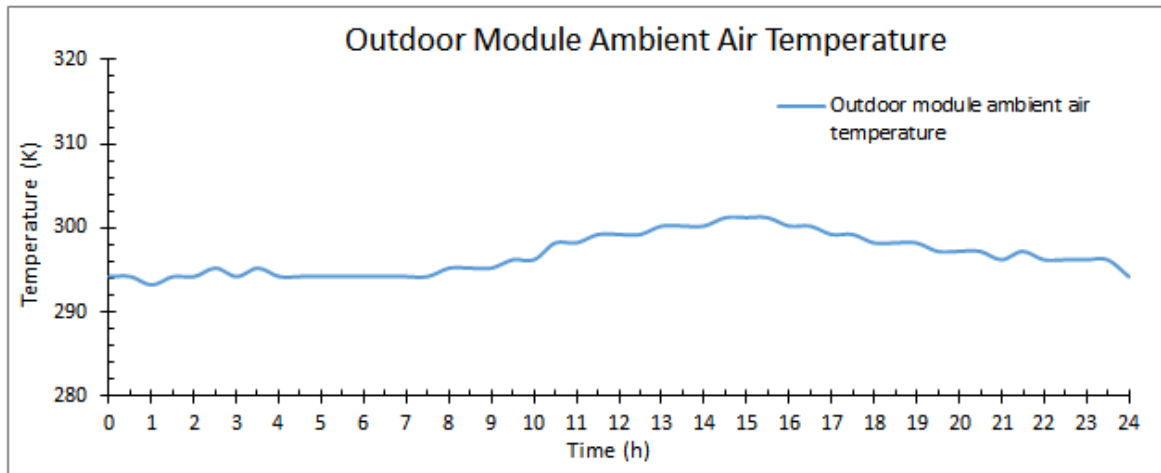
Figure 3.5: Outdoor module ambient air temperature

In this model, the value of ambient air temperature at every time step was obtained by interpolating the air temperature values using "interplq" function in "MATLAB. Initial temperature was set to 294 K. A fixed time step size of 300 s was considered for a total of 288 time steps.

4. *Outdoor PV/PCM Module*

The fourth and last 1-D model implemented with the "MATLAB" environment simulates using the FVM the outdoor experiment carried out by Park et al. (2014) on a PV/PCM module. The model consists of five layers (Figure 3.6) distributed as follows: glass, polycrystalline silicon, front aluminum, paraffinic hydrocarbon, and back aluminum. The thickness and number of elements, layer thickness, and the number of nodes (grid points) for each layer are shown in Table 3.5 below.

Figure 3.6: Outdoor PV/PCM module 1-D model

Table 3.5: Layers properties of the outdoor PV/PCM module 1-D model

layer name	layer thickness (mm)	number of nodes in the layer	number of elements in the layer	thickness of each element in the layer (mm)
glass	2.5	9	9	0.313
polycrystalline silicon	2.5	9	8	0.313

front aluminum	2	7	6	0.333
paraffinic hydrocarbon	50	2	1	50
back aluminum	2	7	7	0.333

The models applied for solar radiation, external convection, absorption, and

transmission were typical to those used in modeling the outdoor PV module. Also, the same

ambient air temperature distribution was used for both models. In the mushy zone, melting

occurs in the paraffinic hydrocarbon layer at a constant temperature T_m. It was modeled by

altering the TDMA algebraic equations in this layer to include the rate of change of latent

energy in the source term as follows:

The source term of the TDMA algebraic equations used in the paraffinic hydrocarbon layer

was computed as shown in Equation (3.22) when $T_{PCM} < T_m$ or $T_{PCM} > T_m$.

$$d_{PCM}(i) = \frac{\rho c p (\Delta x)}{\Delta t} T_{PCM}(i)^0 \qquad (3.22)$$

On the other hand, the latter source term was calculated as shown in Equation (3.23) when

$T_{PCM} = T_m$.

$$d_{PCM}(i) = a_{PCM}(i) T_{PCM}(i)^0 - b_{PCM}(i) T_{balu}(1)^0 - c_{PCM}(i) T_{falu}(Ne\_falu)^0 \qquad (3.23)$$

$$rate\_change\_latent(i) = -d_{PCM}(i) \qquad (3.24)$$

$$rate\_change\_latent(i) = \frac{\partial}{\partial t}(\rho \Delta H) = \frac{\partial}{\partial t}(\rho \beta L) = \rho L \frac{\Delta \beta}{\Delta t} = \rho L \frac{(\beta - \beta^0)}{\Delta t} \qquad (3.25)$$

$$\beta = \beta^0 + \frac{rate\_change\_latent(i)\Delta t}{\rho L} \qquad (3.26)$$

where ρ, cp, L, Δt, Δx, Tm, β, and β^0 are the density, specific heat, heat of fusion, time step

size, element size, melting temperature, element liquid fraction at the current time step, and

element liquid fraction at the previous time step respectively in the paraffinic hydrocarbon layer. $a_{PCM}(i), b_{PCM}(i), c_{PCM}(i), and\ d_{PCM}(i)$ are the coefficients of the algebraic equation for PCM element (i), coefficient of the element after PCM element (i), coefficient of the element before PCM element (i), and the source term of PCM element (i), while $T_{PCM}(i)^0, T_{balu}(1)^0, T_{falu}(Ne\_falu)^0$ are, respectively, the previous time step temperatures of the PCM element (i), first element in the back aluminum layer (i.e. the element just after the last PCM element), and the last element in the front aluminum layer (i.e. the element just before the first PCM element).

The ambient air temperature was calculated by interpolating the air temperature values depicted in Figure 3.5 using "interplq" function in "MATLAB at every time step. The temperature field was initialized to 294 K. The number of time steps considered was 288 each having a fixed size of 300 s.

B. FLUENT

The PV and PV/PCM modules subjected to indoor and outdoor conditions described above and solved numerically as one-dimensional problems using in-house developed codes on "MATLAB" are studied using the "FLUENT" commercial CFD package as three-dimensional objects, as described next.

1. Indoor PV Module

The PV module studied experimentally by Hasan et al. (2010) under indoor conditions and subjected to a radiation flux of magnitude 750 W/m^2 is modeled as a 3-D object using "ANSYS Design Modeler" as shown in Figure 3.7.
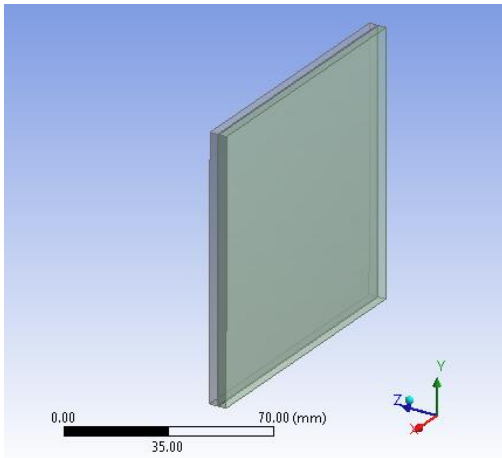
Figure 3.7: Indoor PV module 3-D model geometry created in "ANSYS"
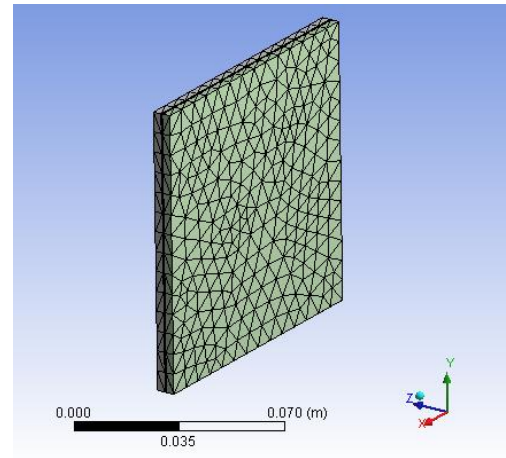
Figure 3.8: Indoor PV module 3-D model mesh created in "ANSYS"

The model consists of a polycrystalline silicon layer embraced by two sheets of transparent Perspex; the dimensions of these three layers are shown in Table 3.6 below.

Table 3.6: Layers dimensions of the indoor PV module "FLUENT" 3-D model

layer name	x-direction dimension (mm)	y-direction dimension (mm)	z-direction dimension (mm)
front perspex	100	100	3
polycrystalline silicon	100	100	0.5
back perspex	100	100	3

31

The mesh of the model shown in Figure 3.8 above was generated using "ANSYS Meshing Software". The advanced sizing function, relevance center, and inflation were set to curvature, fine, and smooth transition respectively. The total number of grid elements was 11520. The thermo-physical properties of perspex and polycrystalline silicon materials used in the model are listed in Table 3.2.

A 3-D double precision session of "FLUENT" was used to simulate the indoor PV module. The unsteady pressure based solver settings were kept at default values such that the gradient computation method is "Green Gauss Cell Based" and the unsteady formulation is "First Order Implicit". Only the "Energy" model was activated because air was not modeled and only the energy equation was required to be solved. Under-relaxation was not employed in the energy equation.

The same boundary conditions applied on the 1-D model of the indoor PV module were extended to the 3-D module. All the boundaries were set to "wall" type. The linearization of the external 750 W/m^2 indoor radiation was carried out in the same manner as in the 1-D model of the indoor PV module such that the resulting external emissivity ε and external radiation source temperature T_{ext} values were 0.3869 and 430 K respectively. These values were directly used in the "mixed" thermal boundary condition applied in "FLUENT" at the front patch along with heat transfer coefficient and free stream temperature values of 8 W/m^{2}K and 293.15 k respectively. A thermal boundary condition of "convection" type was applied at all other boundaries with the same values of free stream temperature and heat transfer coefficient as those introduced into the front boundary patch. The heat transfer coefficient value is based on the same assumption of forced air convection presented above

for the 1-D model of the indoor PV module. The initial temperature was set to 283 K. The model was run using a fixed time step with value of 10s for 600 time steps.

2. *Indoor PV/PCM Module*

"ANSYS Design Modeler" was used to draw the 3-D geometry of the indoor PV/PCM module investigated experimentally by Hasan et al. (2010) as shown in Figure 3.9.
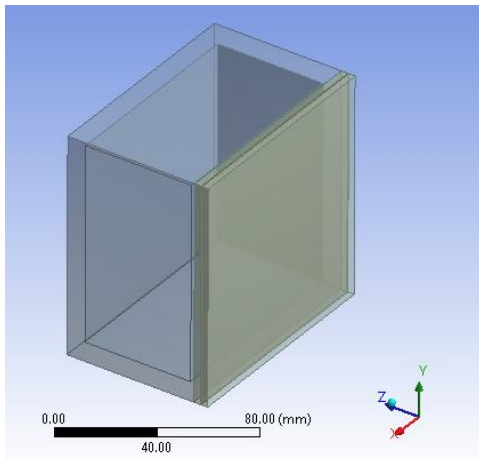
Figure 3.9: Indoor PV/PCM module 3-D model geometry created in "ANSYS"
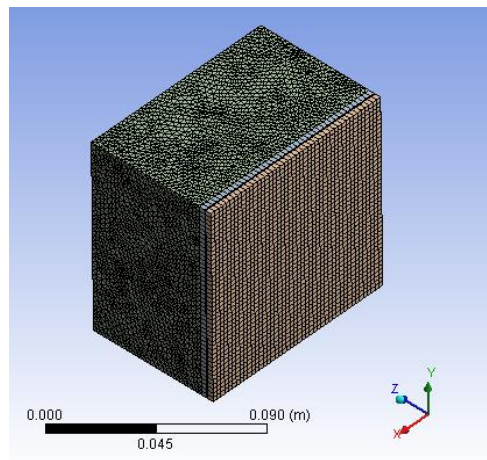
Figure 3.10: Indoor PV/PCM module 3-D model mesh created in "ANSYS"

Five parts constitute this model. The two perspex layers enclosing the polycrystalline silicon layer were attached to an aluminum enclosure of 5 mm thickness. The latter enclosure was filled with a phase change material paraffin wax (RT 20). The dimensions of these parts are shown in Table 3.7.

Table 3.7: Parts dimensions of the indoor PV/PCM module "FLUENT" 3-D model

part name	x-direction dimension (mm)	y-direction dimension (mm)	z-direction dimension (mm)
front perspex	100	100	3
polycrystalline silicon	100	100	0.5
back perspex	100	100	3
aluminum enclosure	100	100	60
paraffin wax (RT 20)	90	90	50

"ANSYS Meshing Software" was used to generate the mesh as shown in Figure 3.10. The advanced sizing function, relevance center, and inflation were set to curvature, fine, and smooth transition respectively. The resulting number of elements was 201247. The thermo-physical properties of the model materials perspex, polycrystalline silicon, aluminum, and paraffin wax are listed above in Table 3.2.

The model's mesh was loaded to "FLUENT" after it was set to 3-D and double precision. Default settings of the gradient computation method and unsteady formulation of the unsteady pressure based solver were maintained at "Green Gauss Cell Based" and "First Order Implicit" respectively. Only the "solidification/melting" model with a "Mushy Zone Constant" of 100000 was activated beside the "Energy" model. Since air was not modeled and weak natural convection currents exist in the paraffin wax region, only the energy equation was solved. The energy equation was not under-relaxed.

The same boundary conditions used with the 3-D indoor PV module were applied on this model except for the heat transfer coefficient which was set at 3 W/m²K based on the same

assumption of natural air convection explained above for the 1-D model of the indoor

PV/PCM module. The temperature was initialized to 283 K. Again, the time step was fixed

and assigned a value of 30 s and computations were performed for a total of 720 time steps.

3. *Outdoor PV Module*

The geometry of the 3-D outdoor PV module studied experimentally by Park et al.

(2014) was plotted using "ANSYS Design Modeler" as shown in Figure 3.11.
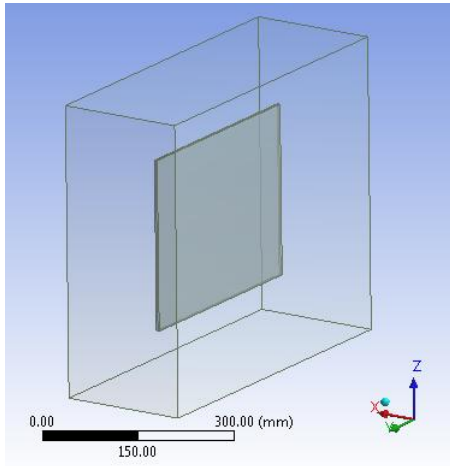
Figure 3.11: Outdoor PV module 3-D model geometry created in "ANSYS"
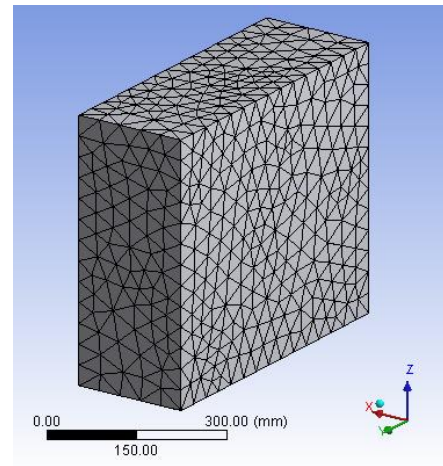
Figure 3.12: Outdoor PV module 3-D model mesh created in "ANSYS"

Table 3.8: Parts dimensions of the outdoor PV module "FLUENT" 3-D model

Part name	x-direction dimension (mm)	y-direction dimension (mm)	z-direction dimension (mm)
glass	2.5	350	280
polycrystalline silicon	2.5	350	280
air	205	550	480

The model of the outdoor PV module is composed of two layers of glass and polycrystalline silicon that are surrounded by an air enclosure extending 100 mm from all sides of the PV layers. The dimensions of the different parts are shown in Table 3.8. Figure 3.12 depicts the mesh of the model that was generated using "ANSYS Meshing Software". The advanced sizing function, relevance center, and inflation were set to curvature, coarse, and smooth transition respectively. A total of 25403 elements were generated. Table 3.2 presents the thermo-physical properties of air, glass, and polycrystalline silicon.

The modal was simulated in a 3-D double precision session of "FLUENT". Typical default settings of the unsteady solver were used such that it was of the pressure based type while a "First Order Implicit" scheme was used for the discretization of the transient term and the gradient was calculated based on the "Green Gauss Cell" method. "Energy" model was used along with a laminar viscous model to model the flow in the air region. "Solar Load" which is one of the "Radiation" models in "FLUENT" was used to account for the solar insolation hitting the front surface of the outdoor PV module.

a. "Solar Load" Model

The "Solar Load" model was set to "Solar Ray Tracing" option. The solar load was updated at every time step. The same analysis and assumptions made for the solar radiation experienced by the 1-D model of the outdoor PV module were implemented for this model. Hence, the values of direct normal radiation and diffuse radiation that are shown in Figure 3.4 were used to obtain piece-wise linear relations for the "Solar Load Illumination Parameters", "Direct Solar Irradiation", and "Diffuse Solar Irradiation", respectively. A "Spectral Fraction" value of 0.4 was used and the default value of 0.3 for ground reflectivity

was maintained. The "Sun Direction Vector" was computed using the "Solar Calculator" whose parameters were set according to the experiment conducted by Park et al. (2014); "Longitude", "Latitude", "Timezone", "Day", "Month", "Hour", and "Minute" fields were set to 126.65, 37.38, 9, 15, 6, 0, and 0 respectively. The default settings of "Fair Weather Conditions" as a "Solar Irradiation method" and a "Sunshine Factor" value of 1 were maintained. The "Grid Orientation" "North" and "East" vectors were set to (1, 0, 0) and (0, -1, 0) respectively to ensure that the PV module faces south direction as stated by Park et al. (2014).

The external convection model applied in the 1-D PV module case was employed in this model; consequently, air velocity has a magnitude of 3.61 m/s and is oriented in the south-east direction. Based on the grid orientation that was set in the solar calculator, the south and east directions lie at the negative x-axis and negative y-axis of the model's geometry respectively; as a result, the air velocity vector was written as (-2.5534, -2.5534, 0). All the boundaries of the model belong to the air region. Due to the south-east direction of the air velocity, the boundaries normal to the negative x and negative y axes were set to be of the "pressure-outlet" type with a 0 pa gauge pressure. The other four boundaries were set to the "velocity-inlet" type such that the "Velocity Specification Method" was set to "components" and the air velocity vector (-2.5534, -2.5534, 0) was used. The same ambient air temperature distribution used in the 1-D model of the PV module and depicted in Figure 3.5 was implemented in "FLUENT" as a user defined function that was used in the two "Thermal" fields "Backflow Total Temperature" and "Temperature" of the "pressure-outlet" and "velocity-inlet" boundary conditions respectively. All interface walls were set to a coupled thermal condition. No boundary was set to participate in the "Solar Ray Tracing".

Only the interface wall between air and glass could participate in the "Solar Ray Tracing".
The type of the latter interface was considered "semi-transparent"; the values of all types
("Direct Visible", "Direct IR", and "Diffuse Hemispherical") of absorptivity and
transmissivity were set to 0.05 and 0.76 respectively based on the same previous assumption
done for the 1-D PV module. Both the "Flow" and "Energy" equations were solved in this
model and the default "SIMPLE" algorithm was used for the "Pressure-Velocity Coupling".
While the "First Order Upwind" scheme was used for the discretization of both the
"Momentum" and "Energy" equations, the "Standard" scheme was used for the discretization
of the "Pressure" equation. No under-relaxation was needed for "Density", "Body Forces",
and "Energy"; however, the under-relaxation factors for the "Pressure" and "Momentum"
equations were set to 0.3 and 0.5 respectively. Temperature and velocity vector fields in the
domain were initialized to 294 k and (-2.5534, -2.5534, 0) respectively. The model was
simulated under a fixed "Time Stepping Method" for 288 time steps each having a size of
300 s.

4. *Outdoor PV/PCM Module*

Using "ANSYS Design Modeler", the 3-D geometry of the PV/PCM module tested
by Park et al. (2014) was drawn as shown in Figure 3.13.
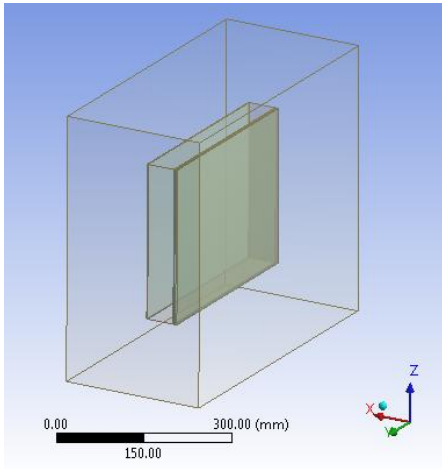
Figure 3.13: Outdoor PV/PCM module 3-D model geometry created in "ANSYS"
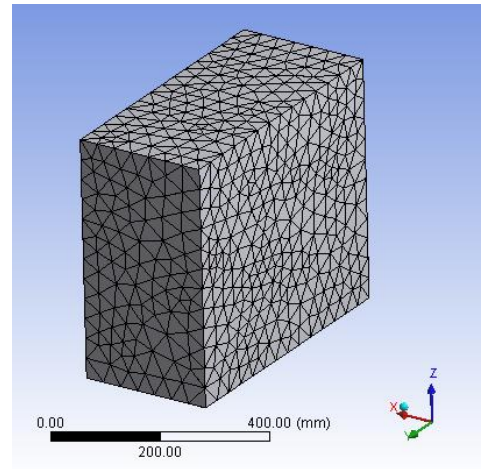
Figure 3.14: Outdoor PV/PCM module 3-D model mesh created in "ANSYS"

Table 3.9: Parts dimensions of the outdoor PV/PCM module 3-D model

Part name	x-direction dimension (mm)	y-direction dimension (mm)	z-direction dimension (mm)
glass	2.5	350	280
polycrystalline silicon	2.5	350	280
front aluminum	2	350	280
paraffinic hydrocarbon	50	350	280
back aluminum	2	350	280
air	259	550	480

The model is made up of six parts. The two PV layers glass and polycrystalline silicon were attached to the phase change material paraffinic hydrocarbon which was placed between two aluminum plates each of 2 mm thickness. An air enclosure that extends 100 mm from all sides of the PV/PCM module surrounds all other parts. Table 3.9 shows the dimensions

39

of the model's parts. "ANSYS Meshing Software" was employed to generate the mesh of the model as depicted in Figure 3.14. The advanced sizing function, relevance center, and inflation were set to curvature, coarse, and smooth transition respectively. The mesh was discretized to 25445 elements. The thermo-physical properties of the model's materials air, glass, polycrystalline silicon, aluminum, acrylic, and paraffinic hydrocarbon are shown above in Table 3.2.

"FLUENT" was set to 3-D double precision mode to run the model case. The various default settings of the unsteady solver were maintained. The pressure based mode was activated. The transient term was discretized based on a "First Order Implicit" scheme and the "Green Gauss Cell Based" method was used to compute the gradient. Beside the "Energy" model, the "solidification/melting" model was activated with its "Mushy Zone Constant" set to 100000. "Solar Ray Tracing" mode was activated in "FLUENT" "Radiation" sub-model "Solar Load" to model the effect of solar insolation at the front of the outdoor PV/PCM module. Also, the laminar viscous model was activated to account for the flow effects in the air region.

The same settings and parameters previously used for the "Solar Load" in the 3-D outdoor PV module were implemented in this model. Also, modeling of the external convection was approached in the same manner in the two models. The six boundaries of the model lie in the air region. Their types and settings were typical to those set previously in 3-D outdoor PV module case. Similarly, all the interface walls including the air-glass interface which was the only wall allowed to participate in the "Solar Ray Tracing" had the same settings and parameters of the interface walls of the 3-D model of the outdoor PV module except for the air-paraffinic hydrocarbon interface wall; at this interface, a wall thickness of 5 mm was

added beside the "Coupled" thermal option and the interface material was set to acrylic in order to account for the thermal effect of the insulation material from which the sides of the paraffinic hydrocarbon container are made of as mentioned by Park et al. (2014). "Flow" and "Energy" equations were solved simultaneously and the "Pressure-Velocity Coupling" was set to the default "SIMPLE" algorithm. The discretization convection scheme employed in the "Momentum" and "Energy" equations was "First Order Upwind"; however, a "Standard" scheme was used for the discretization of the "Pressure" equation. Under-relaxation factors of all equations were set to unity except the "Pressure", "Momentum", and "Liquid Fraction Update" equations for which the under-relaxation factors were set 0.3, 0.5, and 0.9 respectively. Initial values of temperature and velocity vector fields were set to 294 k and (-2.5534, -2.5534, 0) respectively. The "Time Stepping Method" was chosen to be fixed and the time step size was set to 300 s. The model was run for 288 time steps.

C. OPENFOAM

The open source computational fluid dynamics tool box "OpenFOAM" was employed to create and solve numerically 3-D models of all the indoor and outdoor modules considered. "OpenFOAM" includes a wide range of features that can simulate many engineering problems including complex fluid flows that involve turbulence and heat transfer. All these features are coded in C++ and can be customized to meet the requirements of any problem under study. While "OpenFOAM v3.0.1" which is distributed by "The OpenFOAM Foundation" was used for simulating the indoor modules, "OpenFOAM v3.0+" that is released by "OpenCFD Ltd" was employed for running the outdoor modules cases because it contains a model for the solar radiation. Mesh conversion utilities in "OpenFOAM" such

as "fluent3DMeshToFoam" were not used since the cases considered contained multiple regions and these utilities when applied for such cases did not conserve the zoning of the regions. Hence, "OpenFOAM" primitive mesh generator "blockMesh" was utilized to establish the grids. The "blockMesh" is defined in a single dictionary file called "blockMeshDict" and generates hexahedral blocks.

1. *Indoor PV Module*

"blockMesh" was used to create the mesh of the 3-D model of the indoor PV module studied experimentally by Hasan et al. (2010) in a controlled indoor environment where it was subjected to 750 W/m^2 radiation. Using multi-block feature of "blockMesh", the computational cost was decreased via reducing the number of elements generated. The mesh depicted in Figure 3.15 below contains 11200 elements. The "topoSet' and "splitMeshRegions" utilities were used to divide the mesh into four layers. While the two perspex layers enclosing the polycrystalline silicon layer constitute the PV cell, an air layer was modeled next to the front perspex layer to allow the activation of the radiation model in "OpenFOAM". The dimensions of these layers are shown in Table 3.10 below. Thermo-physical properties of perspex, polycrystalline-silicon, and air that were used in the model were defined in the "thermophysicalProperties" and "transportProperties" dictionary files and are listed in Table 3.11 below. The "thermoType" types for the fluid and solid regions were set to "heRhoThermo" and "heSolidThermo" respectively.

Table 3.10: Layers dimensions of the indoor PV module "OpenFOAM" 3-D model

layer name	x-direction dimension (mm)	y-direction dimension (mm)	z-direction dimension (mm)
air	100	100	100
front perspex	100	100	3
polycrystalline silicon	100	100	0.5
back perspex	100	100	3

Figure 3.15: Indoor PV module 3-D model mesh created in "OpenFOAM"

Table 3.11: Thermo-physical properties of the materials used in "OpenFOAM" models

	air	Paraffin Wax RT20	Paraffinic Hydrocarbon	Aluminum	Glass	Perspex	Polycrystalline Silicon
"thermophysicalProperties" dictionary							
Number of moles	1	1	1	1	1	1	1
Molar weight (g/mol)	28.9	352	352	26.98	60	100.12	194.57
Thermal Conductivity (W/m.K)	_	_	_	237	1	0.189	148
Dynamic Viscosity (Kg/m.s)	1.8×10^{-5}	0.205	0.205	_	_	_	_
Prandtl number	0.7	2152.5	2152.5	_	_	_	_
Specific Heat Capacity (J/Kg.K)	1000	2100	2100	871	500	1470	677
Density (Kg/m^3)	_	825	820	2719	3000	1190	2330
"transportProperties" dictionary							
Solidus Temperature (K)	_	294.38	298	_	_	_	_
Liquidus Temperature (K)	_	298.88	298	_	_	_	_
Latent Heat (J/Kg)	_	140300	184000	_	_	_	_

Unlike the generic meaning which a solver implies in CFD as the routine which solves the set of algebraic equations, the solver in "OpenFOAM" is the script that identifies the set of equations that are required to be solved in the different regions considered and the associated constants that are required to be read. "OpenFOAM" has several solvers that are

continuously increasing for the different classes of problems. The standard solver "chtMultiRegionFoam" was applied to solve this case. It is a transient solver that involves conjugate heat transfer between multiple solid and fluid regions; it allows the simulation of buoyant and turbulent fluid flows beside solid heat conduction. While the energy equation is solved in its total enthalpy form in both solid and fluid regions, the momentum and pressure equations are only solved in fluid regions. Because radiation in this solver can be only accounted for in the energy equation of the fluid regions as a source term, an air region was modeled in front of the PV module. The type of "radiationModel" is set in "radiationProperties" files; it was set to "opaqueSolid" for the front perspex, polycrystalline silicon, and back perspex regions and to "viewFactor" for the air region. The "constantAbsorptionEmission" was chosen as the "absorptionEmissionModel" for all regions where an emissivity value of 0.87 was set for the front perspex region. Radiation exchange was defined in the air region "boundaryRadiationProperties" file to be limited to the interface wall between the air and front perspex regions. The "viewFactorsGen" utility was implemented in the air region to calculate the View factors based on a face agglomeration array which was obtained via "faceAgglomerate" utility.

In the "system" folder, boundary conditions for all regions are assigned in the "changeDictionaryDict" files; whereas, the schemes used for discretizing the different terms of the equations and the types of numerical solvers that are used to solve the resulting systems of algebraic equations are set in the "fvSchemes" and "fvSolution" files respectively for every region. The boundary conditions for the PV cell in this model were typically the same as those stated for the indoor PV module that was modeled in "FLUENT". The boundary type of all external patches of the front perspex, polycrystalline

silicon, and back Perspex layers was set to be "patch". The thermal boundary condition

"externalWallHeatFluxTemperature" was implemented on all of them with values of

ambient air temperature and heat transfer coefficient 293.15 K and 8 W/m^{2}K respectively.

As an external forced convection current was assumed as stated before in the 1-D model of

the indoor PV module, all the external patches of the air region were considered inlet

except the patch normal to the positive x-axis was defined as outlet. As a result, a

"fixedValue" thermal boundary condition type was defined at all external patches of the air

region except for the outlet patch, an "inletOutlet" boundary type was defined; however, all

these patches had a uniform temperature value of 293.15 K. While all interface walls were

thermally coupled via the "turbulentTemperatureCoupledBaffleMixed" condition, the

interface wall between the air and front Perspex regions was coupled using the

"turbulentTemperatureRadCoupledMixed" thermal boundary condition to allow the PV

module front surface to be subjected to radiation. The previously assumed value of heat

transfer coefficient and Ito (1972) model for forced heat convection were used to calculate

the velocity field in the air region. By assuming a windward air flow in the positive x-axis

direction, air velocity can be calculated using the equations (3.20) and (3.21) shown earlier.

After substituting the value of h by 8 W/m^{2}K, the magnitudes of the surface air velocity u

and the air velocity U will be equal to 0.8 m/s and 3.214 m/s respectively. As the direction

was assumed to be in the positive x-axis, the velocity vector at all external patches of the

air region was consequently set to (3.214, 0, 0) m/s. All these patches had a velocity

boundary type "fixedValue" (inlet boundary type) except for the outlet patch, its velocity

boundary type was defined as "inletOutlet" (outlet boundary type). For the dynamic

pressure "p_rgh", the "fixedValue" type was assigned for the outlet external air patch;

whereas, the "fixedFluxPressure" boundary type was assigned for all other air patches. A value of 100000 Pa was set at all external air patches for "p_rgh". As the pressure equation solves for the dynamic pressure which is used to calculate the total pressure "p", the boundary type for the total pressure was set to "calculated" for all air external patches. The radiative heat flux "Qr" boundary type for all patches in the air region was set to "greyDiffusiveRadiationViewFactor". "OpenFOAM" allows the direct addition of the external 750 W/m^2 indoor radiation that was applied at the front surface of the PV module by substituting this value in the external radiative heat flux field "Qro" of the "Qr" boundary where a uniform value of -750 was assigned to "Qro" field of the "Qr" interface boundary of the air and frontperspex regions. The negative sign is because the external flux leaves the air region and enters the front perspex region. The discretization schemes for all Laplacian terms in all regions were set to "Gauss linear limited corrected 0.333". In general, a "Gauss linear" scheme represents a central differencing scheme. The "Euler" scheme was used to discretize the transient term in all regions. Divergence schemes were only applicable in the air region; they were all set to "Gauss upwind" which is equivalent to a first order upwind scheme. The "PIMPLE" algorithm was employed in the solution process across all regions. While the "PCG" numerical solver was used to solve the system of algebraic equations of the energy equation in the solid regions (front perspex, polycrystalline silicon, and back Perspex), the "PBiCG" solver was used in the air region. The "GAMG" and "PBiCG" solvers were respectively utilized for the pressure and momentum equations governing the air region. All velocity, pressure, and temperature fields were initialized to (3.214, 0, 0) m/s, 100000 Pa, and 283 K respectively. The

47

"OpenFOAM" model was run for 6000 s with a modifiable time step and a maximum allowable courant number of 232.

2. *Indoor PV/PCM Module*

The mesh of the 3-D model of the indoor PV/PCM module was generated in "OpenFOAM" by extending the previously drawn mesh of the indoor PV module via the multi-block feature of "blockMesh" such that a third block which contains the phase change material was added to the two existing blocks. The mesh shown in Figure 3.16 below is made up of 16000 elements. An aluminum enclosure containing phase change material paraffin wax (RT 20) was added to the four layers (air, front perspex, polycrystalline silicon, and back Perspex) previously discussed in the 3-D model of the indoor PV module. The six regions of the model were constructed using "topoSet' and "splitMeshRegions" utilities. Table 3.12 below summarizes the dimensions of these regions.

Table 3.12: Dimensions of the regions of the indoor PV/PCM module "OpenFOAM" 3-D model.

layer name	x-direction dimension (mm)	y-direction dimension (mm)	z-direction dimension (mm)
air	100	100	100
front perspex	100	100	3
polycrystalline silicon	100	100	0.5
back perspex	100	100	3
aluminum enclosure	100	100	60
paraffin wax (RT 20)	90	90	50

Figure 3.16: Indoor PV/PCM module 3-D model mesh created in "OpenFOAM"

Thermo-physical properties of the materials in the six regions of the model were included

in the "thermophysicalProperties" dictionary files; additional properties related to melting

for the fluid regions' materials (air and paraffin wax) were included in the

"transportProperties" dictionary files as shown in Table 3.11 above. The "heRhoThermo"

and "heSolidThermo" were respectively defined as the "thermoType" types for the fluid

and solid regions of the model.

For this model, the "meltFoam" solver was integrated with the standard solver

"chtMultiRegionFoam" discussed earlier to account for melting and solidification in the

phase change material. The obtained solver "chtMultiRegionMeltFoamfour" used solves

the governing equations of the fluid regions in two modes. In the first mode, the latent heat for a fluid (for e.g air) is 0; consequently, the solution in the fluid region is typical to that obtained upon using the standard "chtMultiRegionFoam" solver. In the second mode, the latent heat for a fluid (for e.g paraffin wax) is different than 0; hence, a modified energy equation is used which accounts for melting by explicitly evaluating the transient and convective latent energy terms such that they are added to the source terms of the energy equation. In the "sources' file before solving the energy equation, the change in latent energy is updated as follows:

$$DH = DHnew \qquad (3.27)$$

$$if\ DH(i) > L\ \rightarrow\ DH(i) = L \qquad (3.28)$$

$$if\ DH(i) < 0\ \rightarrow\ DH(i) = 0 \qquad (3.29)$$

$$lf = DH/L \qquad (3.30)$$

where DH, DHnew, lf, and L are respectively the change in latent energy used in the current time step, the change in latent energy computed after solving the energy equation in the previous time step, the liquid fraction in the current time step, and the heat of fusion of the phase change material. Afterwards, in the energy equation "EEqn" file, the latent energy terms are computed as follows:

$$ST = fvc :: ddt(rho, DH),\ \text{such that } ddt(rho, DH) \equiv \frac{\partial}{\partial t}(\rho \Delta H) \qquad (3.31)$$

$$STconv = fvc :: div(phi, DH),\ \text{such that } div(phi, DH) \equiv \nabla.(\rho \boldsymbol{v} \Delta H) \qquad (3.32)$$

Where ST and STconv are respectively the transient and convective latent energy terms. After solving the energy equation, the change in the latent heat of the PCM is updated as follows:

$h = cp{\times}T$ (3.33)

$Tstar = (Tl - Ts){\times}lf + Ts$ (3.34)

$DHnew = DH + omegaDH{\times}(h - cp{\times}Tstar)$ (3.35)

Where h, cp, Tl, and Ts are the sensible enthalpy, specific heat capacity, liquidus

temperature, and solidus temperature of the phase change material respectively; whereas,

omegaDH is a relaxation factor used for computing the change in the latent energy of the

PCM. The pressure and momentum equations are not considered in the solution process of

the second mode since weak convection currents are assumed to be generated in the phase

change materials. The air region was modeled a head of the PV/PCM module to enable

radiation exchange at the front surface of the module. The same radiation settings stated

earlier for all the regions of the indoor PV module had been also employed in this model.

For the paraffin wax region, the "radiation" and "radiationModel" were set to "none";

whereas, an "opaqueSolid" was set for the "radiationModel" in the aluminum region along

with a "constantAbsorptionEmission" type for the "absorptionEmissionModel".

The same boundary conditions, schemes, algorithm, and numerical solvers that were

previously implemented for the solid and fluid regions of the indoor PV module were also

used for the solid and fluid regions in this model except for some adjustments in the

boundary conditions as follows. Based on the natural convection assumption under which

the indoor PV/PCM module was experimented by Hasan et. al (2010) as discussed earlier

in the 1-D model of the PV/PCM module, the heat transfer coefficient field of air in the

"externalWallHeatFluxTemperature" thermal boundary type that was applied on all

external patches of the solid regions was assigned a value of 3 W/m^{2}K. The direction of air

was assumed to be in the positive y-axis and the velocity vector at all external patches of the air region was assumed (0, 0.3, 0) m/s. Hence, only the external patch which is normal to the positive y-axis was defined as an outlet while the remaining external patches of the air region were defined as an inlet. The same discretization schemes that were used in the air region were also implemented in the paraffin wax region. For the latter region, the "PBiCG" solver was assigned to solve the system of algebraic equations of the energy equation which was the only equation governing this fluid region. While the velocity fields in the air and paraffin wax regions were initialized to (0, 0.3, 0) and (0, 0.00008, 0) m/s respectively, all pressure and temperature fields were initialized to 100000 Pa and 283 K respectively. After setting the maximum allowable courant number to 200, this case was simulated in "OpenFOAM" for 21600 s using a modifiable time step.

3. *Outdoor PV Module*

The outdoor PV module was modeled in "OpenFOAM v3.0+" in two separate cases that differ in the way of modelling air around the module. In the first case, the PV module is enclosed inside the air domain while a layer of air is modeled next to the front surface of the PV module in the second case. The two cases were set as follows:

a. Outdoor PV module case 'a'

The mesh of the 3-D model of the outdoor PV module simulated previously in "FLUENT" was regenerated in "OpenFOAM" using "blockMesh". A total number of 21648 elements constitute the model's mesh depicted in Figure 3.17 below. The model which was formed using the "topoSet' and "splitMeshRegions" utilities was composed of

two layers of glass and polycrystalline silicon that were enclosed inside an air region. The

dimensions of these regions are listed in Table 3.13 below.

Table 3.13: Dimensions of the regions of the outdoor PV module "OpenFOAM" 3-D model with an air enclosure.

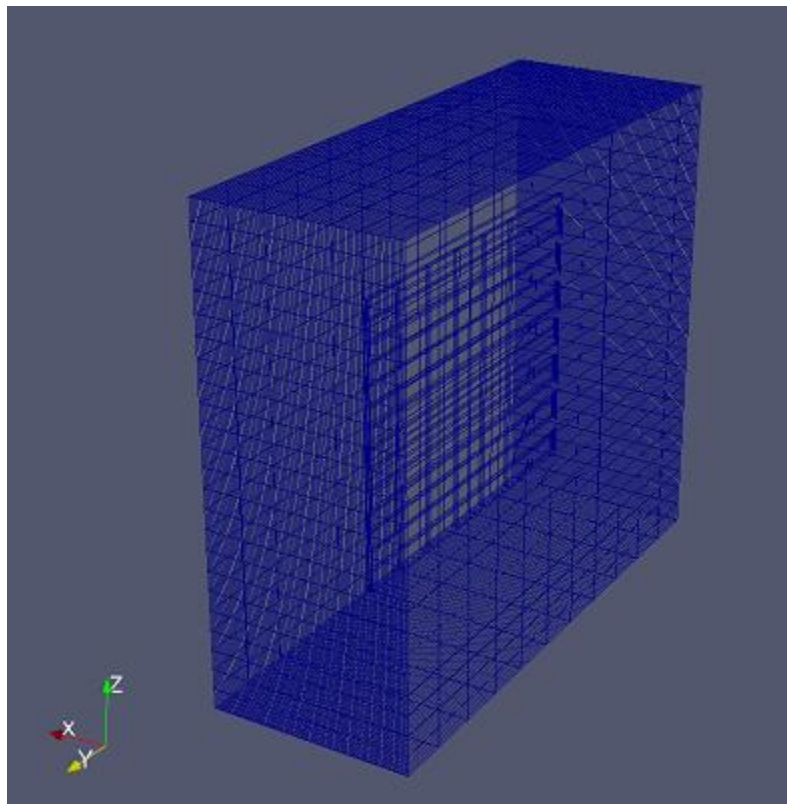| Part name	x-direction dimension (mm)	y-direction dimension (mm)	z-direction dimension (mm)
glass	2.5	350	280
polycrystalline silicon	2.5	350	280
air	205	550	480

Figure 3.17: Outdoor PV module 3-D model mesh (with an air enclosure) created in "OpenFOAM"

Table 3.11 above shows a briefing of the thermos-physical properties of the model's materials that were included in the "thermophysicalProperties" and "transportProperties" dictionary files. The fluid and solid regions were assigned "heRhoThermo" and "heSolidThermo" respectively as "thermoType" types.

The "OpenFOAM" standard solver "chtMultiRegionFoam" that was previously discussed was employed to solve this case. The solar radiation heat exchange is limited to the air fluid region. An "opaqueSolid" "radiationModel" was set for the solid regions glass and polycrystalline silicon. "OpenFOAM v3.0+" is distinguished by its capability of modeling the effects of solar radiation via the "solarLoad" "radiationModel". The solar radiation can be calculated based on several methods including the "Fair Weather Conditions Method" which is employed in the "ASHRAE clear sky model". While the evaluation of the direct, diffuse and reflected components of the solar radiation is done in the "solarLoad" source file based on "ASHRAE clear sky model", the solar angles and the direct normal radiation quantities are computed in the source file of the "solarCalculator" sub model which is associated with the "solarLoad" model. Since the approach which was used for modeling the solar radiation in the 1-D model of the outdoor PV module was also implemented for this model, the existing sub model "solarCalculator" was modified to interpolate with time the values of radiation that were measured by Park et al. (2014) with a shaded pyranometer; consequently, the corresponding direct normal radiation values were computed using equation (3.19) previously shown in the 1-D model of the outdoor PV module. The "solarLoad" model applies the direct normal radiation that is calculated in the "solarCalculator" only on the faces with "hitFacesId" which are determined in a separate "faceShading" model that evaluates the faces which should be hit by solar radiation based

54

on transmissivity values. Because the "faceShading" model was not functioning properly, the "solarLoad" model was modified to ignore the "faceShading" model and loop over all the faces upon applying the solar radiation. Eventually, the solar radiation will be only implemented on the faces of the patches assigned in the "boundaryRadiationProperties" file to participate in the solar radiation. The "solarLoad" model was also adjusted to accommodate the modified sub model. The new "solarLoad" model and corresponding sub model were named "solarLoad_amin2" and "solarCalculator_amin2" respectively. In the "radiationProperties" file of the air region, the "radiationModel" was set to "solarLoad_amin2" and its corresponding settings which were assigned as follows were typical to the solar load model settings that were previously used in the 1-D and 3-D "FLUENT" models of the outdoor PV module. The "sunDirectionModel" was set to "sunDirTracking" to allow the "solarCalculator_amin2" sub model to calculate the solar angles and sun direction. The "localStandardMeridian", "startDay", "startTime", "longitude", and "latitude" fields were set to 9, 166, 0, 126.65, and 37.38 respectively. As for the grid orientation, the "gridUp" vector which represents the north direction was set to (1, 0, 0) while the "gridEast' vector that stands for the east direction was set to (0, -1, 0). Consequently, the negative x-axis and the negative y-axis of the model are assigned the south and east directions respectively and the front surface of the glass layer will be facing south. The "sunLoadModel" type was set to "sunLoadFairWeatherConditions" and the solar diffusivity constant "C" was assigned the value of 0.134 according to "ASHRAE" tables. The ground reflectivity was set to 0.3. The solar load calculations were updated every 90 s. All regions were assigned "constantAbsorptionEmission" as a type for the "absorptionEmissionModel" where a 0.4 absorptivity value was considered for the glass

region. The "boundaryRadiationProperties" file of the air region restricted all the radiation exchange to the interface wall between the air and glass regions. The "viewFactorsGen" utility was implemented in the air region to calculate the View factors based on a face agglomeration array which was attained via "faceAgglomerate" utility.

Velocity and thermal boundary conditions applied for this model's case were typical to those applied for the 3-D "FLUENT" model of the outdoor PV module. The same external convection model and wind direction were employed. In this case, all the external patches of the model belong to the air region and have a velocity vector (-2.5534, -2.5534, 0) m/s. Air velocity was directed in the south-east. Because the negative x and negative y axes were set to represent the south and east directions respectively as described in the grid orientation above, the external patches normal to these axes were assigned an "inletOutlet" velocity boundary type as they were considered as outlets while all other external patches were set to be of the "fixedValue" type as they were considered as inlets. A "groovyBC" thermal boundary condition was implemented on all external patches of this model. The "groovyBC" allows arbitrary specification of boundary conditions based on expressions; it can be installed via separate library called "swak4Foam". A polynomial equation was obtained for the ambient air temperature distribution shown above in Figure 3.5; this equation was employed in the "groovyBC" to establish a thermal boundary condition that varies with time at all the external patches. The polynomial equation terms were defined in the "variables" field of the "groovyBC" as follows:

$"A = -0.00000000000000000000000001939 * \text{pow}(time(\ ), 6); B = 0.00000000000000000000605395772 * \text{pow}(time(\ ), 5); C =$

$-0.0000000000000000069575417418214 * \text{pow}(time(\quad), 4); D =$

$0.00000000000354781274299131 * \text{pow}(time(\quad), 3); E =$

$-0.00000000761250753544829 * \text{pow}(time(\quad), 2); F = 0.000595629457734503 *$

$time(\quad); G = 293.250936624594;"$

The "valueExpression" field was set to $"A + B + C + D + E + F + G"$. To allow the

exposure of the front surface of the PV module to solar radiation, the

"turbulentTemperatureRadCoupledMixed" thermal boundary condition was implemented

at the interface wall between the glass and air regions; thermal coupling between all other

interface walls was attained through the "turbulentTemperatureCoupledBaffleMixed"

condition. The value of the dynamic pressure "p_rgh" was set to 100000 Pa at all air

patches. While the outlet external air patches were assigned a "fixedValue" "p_rgh"

boundary type, a "fixedFluxPressure" type was set for all other air patches. A "calculated"

total pressure "p" type was assigned to all air patches. The boundary type of the radiative

heat flux "Qr" was set to "greyDiffusiveRadiationViewFactor" at all the patches of the air

region, but the "emissivityMode" was set to "solidRadiation" only at the interface wall

between the air and glass regions. While the "Gauss linear corrected" and "Euler"

discretization schemes were respectively employed for the Laplacian and transient terms in

all regions, the "Gauss upwind" divergence scheme was only applied in the air region. The

model was simulated using the "PIMPLE" algorithm for all regions. The numerical solver

"PCG" was used to solve the resulting systems of algebraic equations of the energy

equation governing the solid regions (glass and polycrystalline silicon) and the pressure

equation of the air region. The "PBiCG" solver was assigned to solve the momentum and

energy equations' systems of algebraic equations that govern the air region. The initial values of the velocity, pressure, and temperature fields were respectively set to (-2.5534, -2.5534, 0) m/s, 100000 Pa, and 294 K. After considering a modifiable time step and a maximum allowable courant number value of 232 in the "controlDict" file, the model case was simulated for 86400 s.

b.   Outdoor PV module case 'b'

Another case of the outdoor PV module was modeled in "OpenFOAM v3.0+" by altering the dimension and position of the air region which now extends 400 mm beyond the front surface of the PV module. Figure 3.18 below shows the mesh of the second case which is made up of 16800 elements. The same approach used in the former case for creating the mesh was used in this model in addition to employing the multi-block feature of "blockMesh". A separate block of air region extended beyond the glass and polycrystalline silicon layers which were grouped in a single block. Table 3.14 below lists the dimensions of these regions. The same materials' thermos-physical properties, solver, and radiation settings which were used in the model of the outdoor PV module case 'a' were also employed for this model's case except for modifying the absorptivity value from 0.4 to 0.23 in the "absorptionEmissionModel" of the glass region.
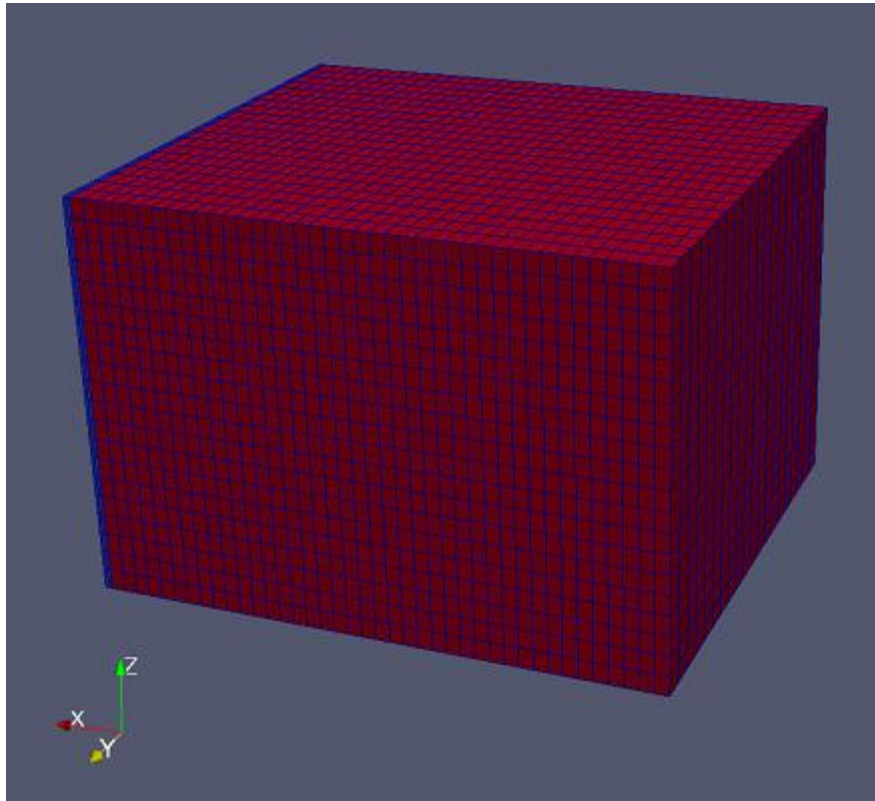
Figure 3.18: Outdoor PV module 3-D model mesh (with air extending beyond the system front surface) created in "OpenFOAM"

Table 3.14: Dimensions of the regions of the outdoor PV module "OpenFOAM" 3-D model with an air region extending beyond the system front surface.

Part name	x-direction dimension (mm)	y-direction dimension (mm)	z-direction dimension (mm)
glass	2.5	350	280
polycrystalline silicon	2.5	350	280
air	400	350	280

Similarly, the same boundary conditions, numerical schemes, numerical solvers, and "controlDict" settings were implemented in both cases except that the external patches were not restricted to the air region anymore in this case; rather, the solid regions glass and polycrystalline silicon had also external patches. In addition, the air region in this case has a single interface wall which is the one with the glass region. The thermal boundary condition "externalWallHeatFluxTemperature" was applied on all external patches of the solid regions with values of ambient air temperature and heat transfer coefficient of 294 K and 8.56 W/m^{2}K respectively. The value of heat transfer coefficient was typical to that used in the 1-D model of the outdoor PV module.

4. Outdoor PV/PCM Module

Based on the outdoor PV module cases previously presented, two separate cases were established to model the outdoor PV/PCM module in "OpenFOAM v3.0+" as follows.

a. Outdoor PV/PCM module case 'a'

The mesh for this case was typical to that created for the 3-D model of the outdoor PV/PCM module studied earlier in "FLUENT". "blockMesh" was utilized to generate the model's mesh (Figure 3.19) which was composed of 27456 elements. It represents an extension of the previously studied outdoor PV module case 'a' such that the phase change material paraffinic hydrocarbon that was contained between two aluminum plates was added at the back of the PV module. The "OpenFOAM" utilities "topoSet' and "splitMeshRegions" were employed to create the model's six regions (air, glass, polycrystalline silicon, front aluminum, paraffinic hydrocarbon, and back aluminum)

whose dimensions are shown in Table 3.15 below. The "thermophysicalProperties"

dictionary files contained the thermo-physical properties of the materials used in the

different regions of the model beside the "transportProperties" dictionary files which

included melting related properties for the fluid regions materials (air and paraffinic

hydrocarbon); these properties were described in Table 3.11 above. The "thermoType" for

the fluid and solid regions in this case were assigned the "heRhoThermo" and
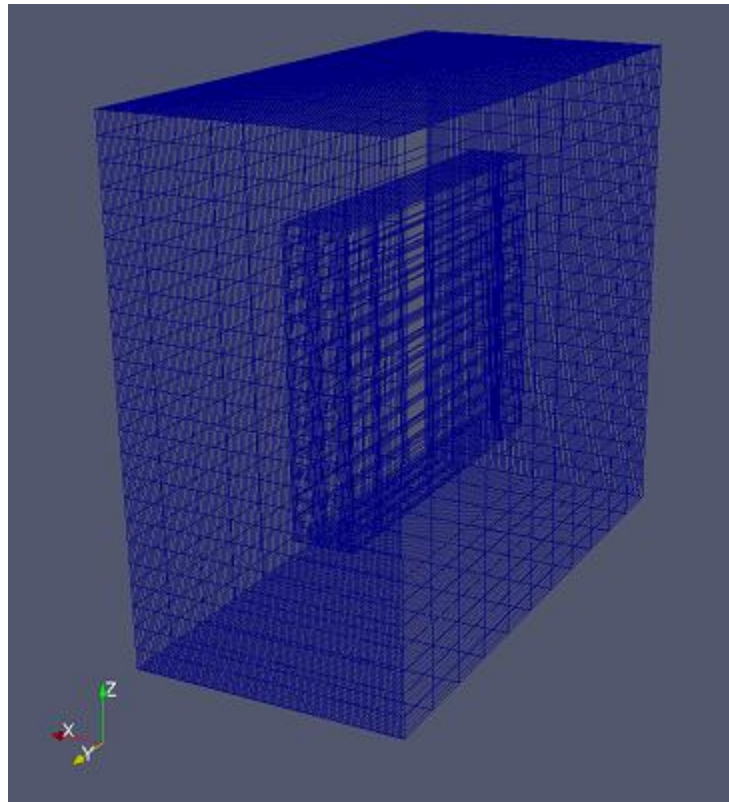
"heSolidThermo" types respectively.

Figure 3.19: Outdoor PV/PCM module 3-D model mesh (with an air enclosure) created in "OpenFOAM"

Table 3.15: Dimensions of the regions of the outdoor PV/PCM module "OpenFOAM" 3-D model with an air enclosure.

Part name	x-direction dimension (mm)	y-direction dimension (mm)	z-direction dimension (mm)
glass	2.5	350	280
polycrystalline silicon	2.5	350	280
front aluminum	2.5	350	280
paraffinic hydrocarbon	50	350	280
back aluminum	2.5	350	280
air	260	550	480

The "chtMultiRegionMeltFoamfour" solver that accounts for melting as illustrated earlier in the 3-D "OpenFOAM" model of the indoor PV/PCM module was also employed in this case. The radiation settings previously made for the air, glass, and polycrystalline silicon regions in the outdoor PV module case 'a' including assigning "solarLoad_amin2" as a "radiationModel" type for the air region were also used in this case. In the front aluminum and back aluminum regions the "radiationModel" was set to "opaqueSolid" and the "absorptionEmissionModel" was assigned a "constantAbsorptionEmission" type. On the other hand, the "radiation" and "radiationModel" were set to "none" for the paraffinic hydrocarbon region.

The same boundary conditions, algorithm, and numerical solvers that were implemented earlier for the air and solid regions in the outdoor PV module case 'a' were also used in this case. The "Gauss linear limited corrected 0.333" discretization scheme was assigned for all Laplacian terms for the front aluminum, back aluminum, and paraffinic hydrocarbon regions while the "Euler" scheme was employed for the transient term in these

regions. The divergence term in the paraffinic hydrocarbon region was discretized using the "Gauss upwind" scheme. The system of algebraic equations of the energy equation governing the paraffinic hydrocarbon region was solved using the "PBiCG" solver while the "PCG" solver was employed to solve that system of equations in the front aluminum and back aluminum regions. The initial velocity fields in the air and paraffinic hydrocarbon regions were assigned the vectors (-2.5534, -2.5534, 0) and (0, 0.00002, 0) m/s respectively. The pressure and temperature fields were respectively initialized to 100000 Pa and 294 K. In the "controlDict" file, the value of maximum allowable courant number was set to 232, a modifiable time step was used, and the end time of the case was set to 86400 s.

b. Outdoor PV/PCM module case 'b'

Again, the location and dimensions of the air region were modified to establish the second case of the outdoor PV/PCM module in "OpenFOAM v3.0+". The mesh of the outdoor PV/PCM module case 'b' was generated in "blockMesh" using the multi-block feature. Three blocks were created in the geometric domain. The first block contains the air region which extends 400 mm beyond the glass layer. The second block contains the glass and polycrystalline silicon layers while the paraffinic hydrocarbon PCM region was included in the final block along with the two aluminum plates surrounding it. The mesh was composed of 27600 elements (Figure 3.20). Table 3.16 below shows the dimensions of the model's regions: air, glass, polycrystalline silicon, front aluminum, paraffinic hydrocarbon, and back aluminum. These regions were established via "topoSet' and "splitMeshRegions" utilities in "OpenFOAM".
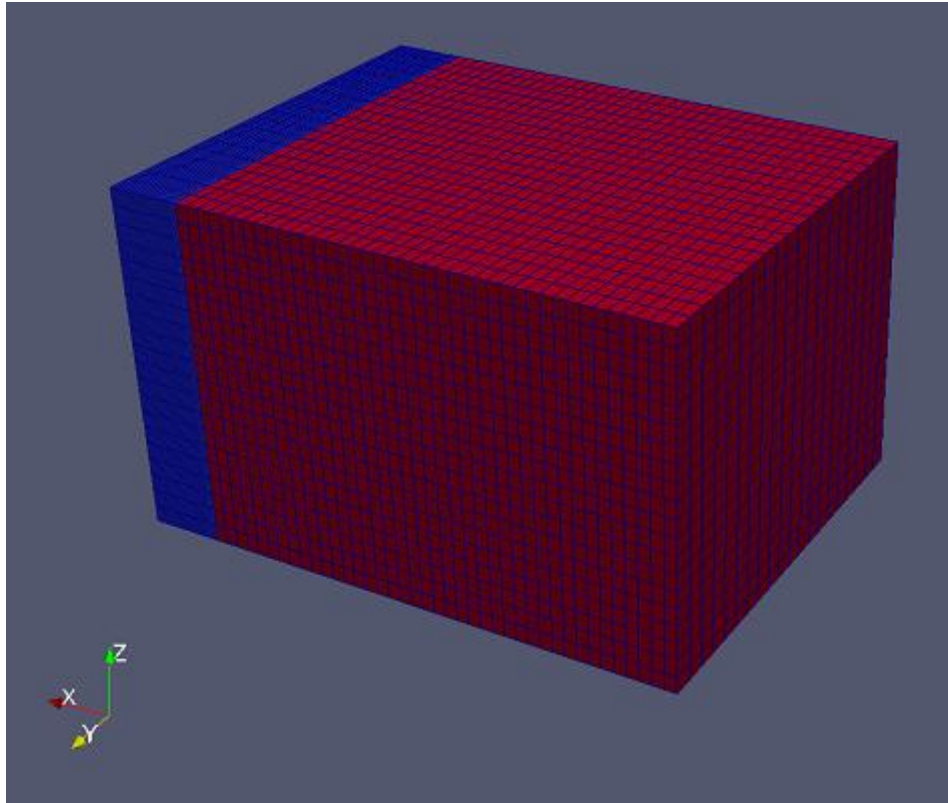
Figure 3.10: Outdoor PV/PCM module 3-D model mesh (with air extending beyond the system front surface) created in "OpenFOAM"

Table 3.16: Dimensions of the regions of the outdoor PV/PCM module "OpenFOAM" 3-D model with an air region extending beyond the system front surface.

Part name	x-direction dimension (mm)	y-direction dimension (mm)	z-direction dimension (mm)
glass	2.5	350	280
polycrystalline silicon	2.5	350	280
front aluminum	2	350	280
paraffinic hydrocarbon	50	350	280
back aluminum	2	350	280
air	400	350	280

The thermos-physical properties of the materials of the outdoor PV/PCM module case 'a' model as well as its solver and radiation settings were kept the same in this model's case except for the absorptivity value in the "absorptionEmissionModel" of the glass region which was changed from 0.4 to 0.23.

Moreover, identical settings of the "controlDict" file, numerical schemes, numerical solvers, and initial values across all regions were used in both cases. Also, the boundary conditions employed in the outdoor PV/PCM module case 'a' were preserved in this case except for few modifications as follows. All the regions of the model had external patches and the only interface wall with the air region is at the glass region. While the thermal boundary conditions of the external patches of the air region were typically the same as those used in the previous case, an "externalWallHeatFluxTemperature" thermal boundary condition was implemented at the external patches of all other regions. The ambient air temperature and heat transfer coefficient were assigned the values of 294 K and 8.56 W/m^{2}K respectively. The value of heat transfer coefficient used was based on the external convection model previously illustrated in the 1-D model of the outdoor PV module.

CHAPTER IV

RESULTS

A. MATLAB

In all "MATLAB" cases, temperature at the first node of the model was saved for all time steps to be compared with the corresponding front surface temperature profile provided by Hasan et al. (2010) and Park et al. (2014).
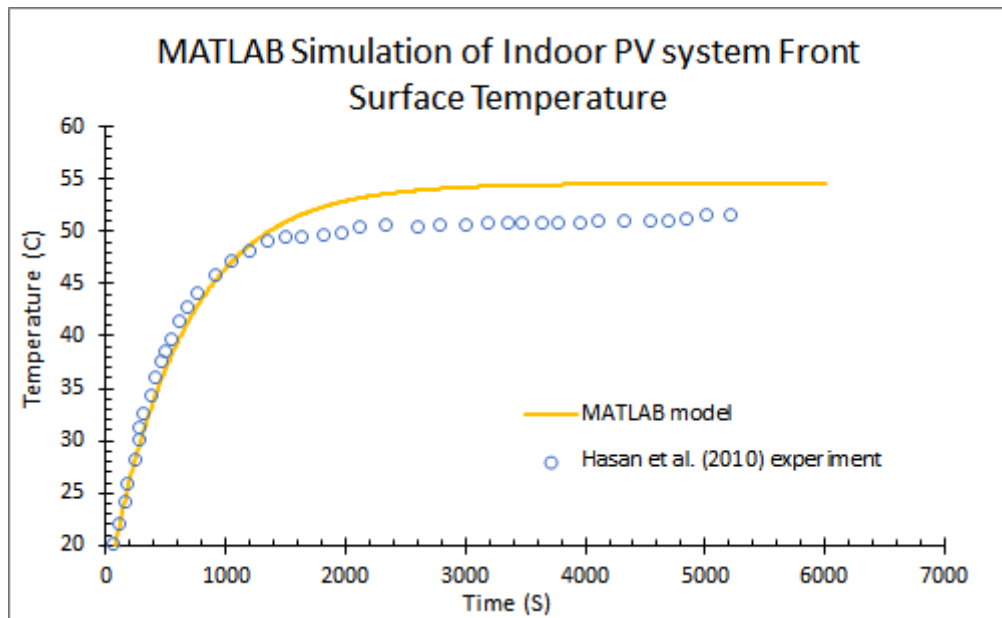
1. Indoor PV Module

Figure 4.1: front surface temperature of the 1-D model of the indoor PV module simulated in "MATLAB"

Figure 4.1 above shows that the difference between the front surface temperature of the 1-D model of the indoor PV module simulated in "MATLAB" and that obtained experimentally by Hasan et al. (2010) does not exceed 3.7 ℃.
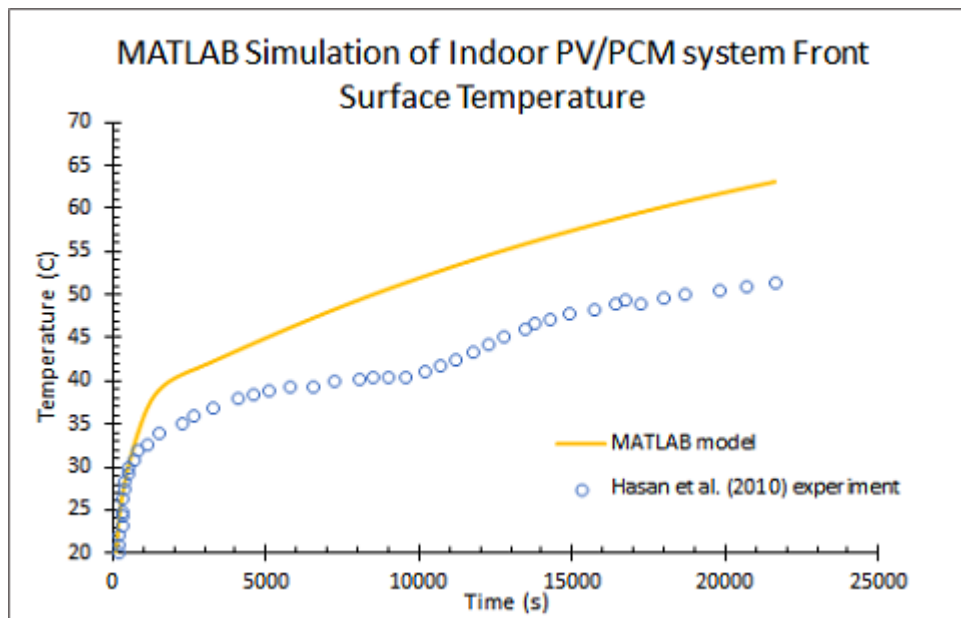
2. *Indoor PV/PCM Module*

Figure 4.2: front surface temperature of the 1-D model of the indoor PV/PCM module simulated in "MATLAB"

A large discrepancy of about 11.5 ℃ can be noted above in Figure 4.2 in the front surface temperature values of the 1-D model of the indoor PV/PCM module when compared with the corresponding experimental values from Hasan et al. (2010).
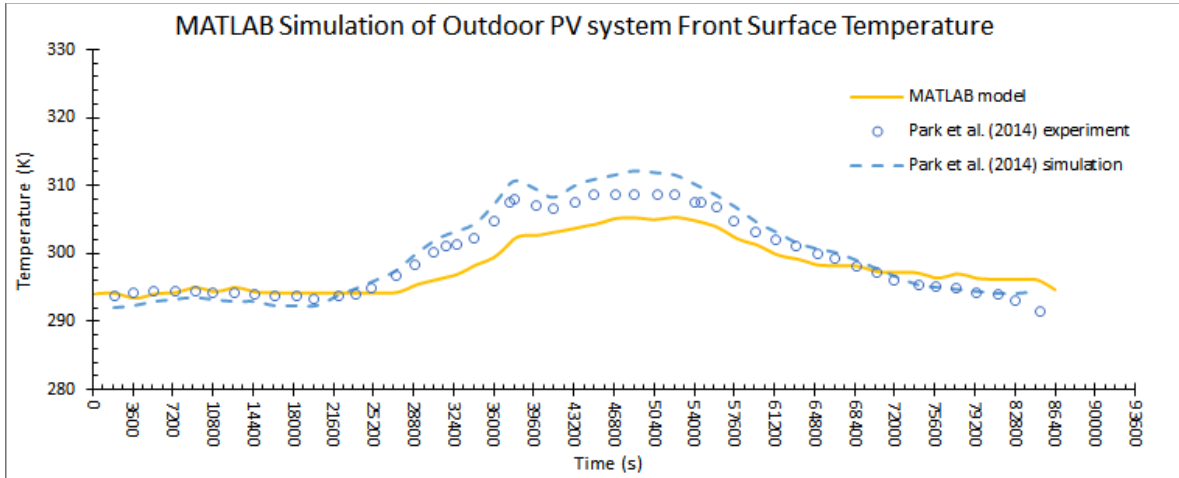
3. *Outdoor PV Module*

Figure 4.3: front surface temperature of the 1-D model of the outdoor PV module simulated in "MATLAB"

The front surface temperature distribution of the 1-D model of the outdoor PV module depicted above in Figure 4.3 has a profile similar to that of Park et al. (2014) experimental temperature distribution; however, it shows a maximum difference of 6 K at 37800 s.
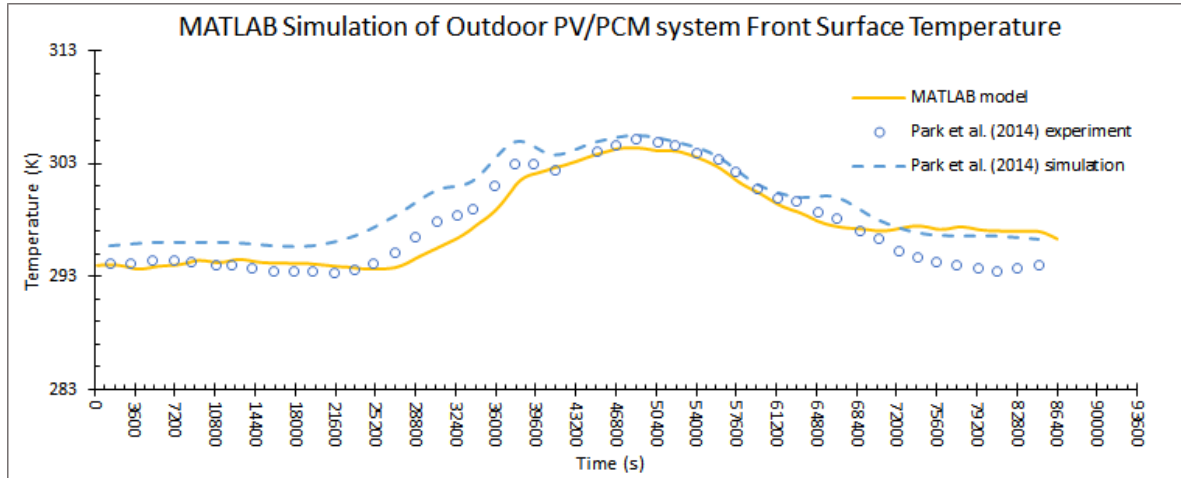
4. *Outdoor PV/PCM Module*

Figure 4.4: front surface temperature of the 1-D model of the outdoor PV/PCM module simulated in "MATLAB"

The "MATLAB" simulation of the 1-D model of the outdoor PV/PCM module shown in Figure 4.4 above results in a maximum discrepancy of 3.7 K from the experimental temperature data towards the end of the 24 hours; however, the "MATLAB" simulation exhibits a better overall proximity to the experimental result when compared to the simulation performed by Park et al. (2014).

B. FLUENT

For every "FLUENT" 3-D model, a surface monitor that reports the area weighted average static temperature was created. The monitor was applied at the module's front surface and recorded the temperature value at every time step. The latter results were

compared with the corresponding experimental results obtained by Hasan et al. (2010) and Park et al. (2014) as follows.
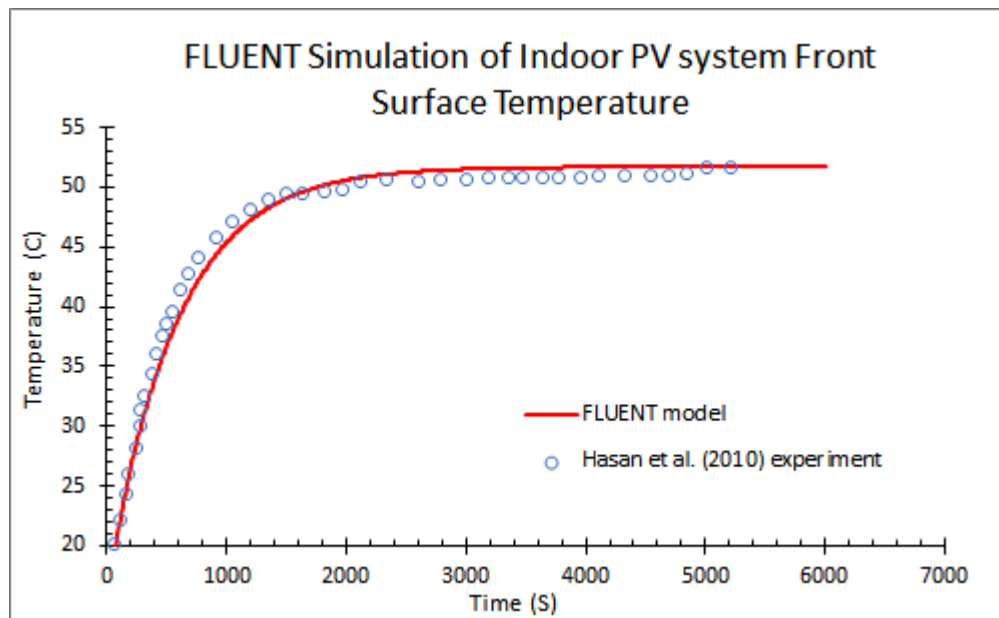
1. *Indoor PV Module*

Figure 4.5: front surface temperature of the 3-D model of the indoor PV module simulated in "FLUENT"

The front surface temperature of the 3-D model of the indoor PV module obtained using "FLUENT" is very close to data measured by Hasan et al. (2010) in his experiment as shown in Figure 4.5 above.
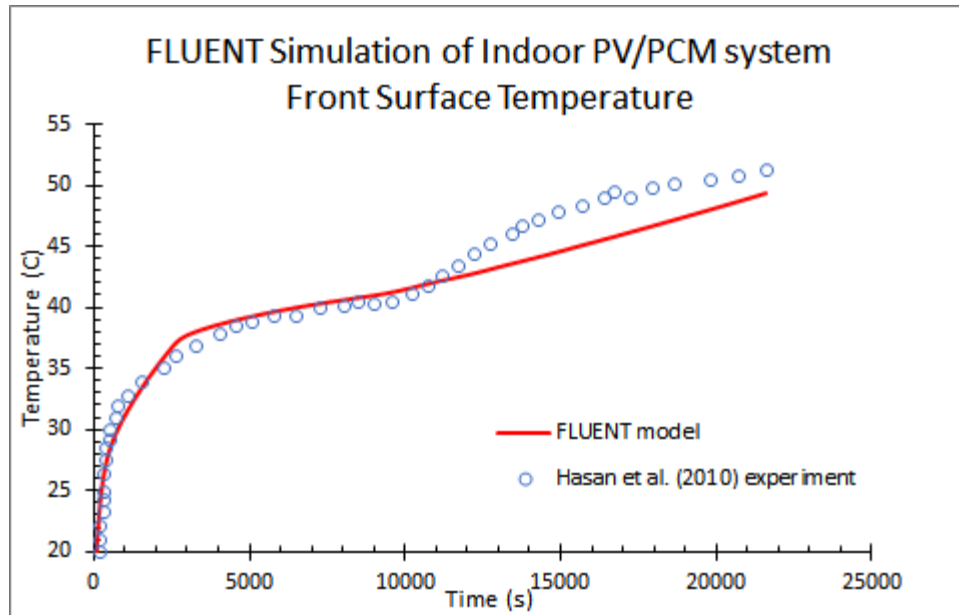
2. *Indoor PV/PCM Module*

Figure 4.6: front surface temperature of the 3-D model of the indoor PV/PCM module simulated in "FLUENT"

The maximum discrepancy between the "FLUENT" simulation and Hasan et al.

(2010) experimental results regarding the front surface temperature of the 3-D model of the

indoor PV/PCM module does not exceed 3.7 ºC as shown in Figure 4.6 above.
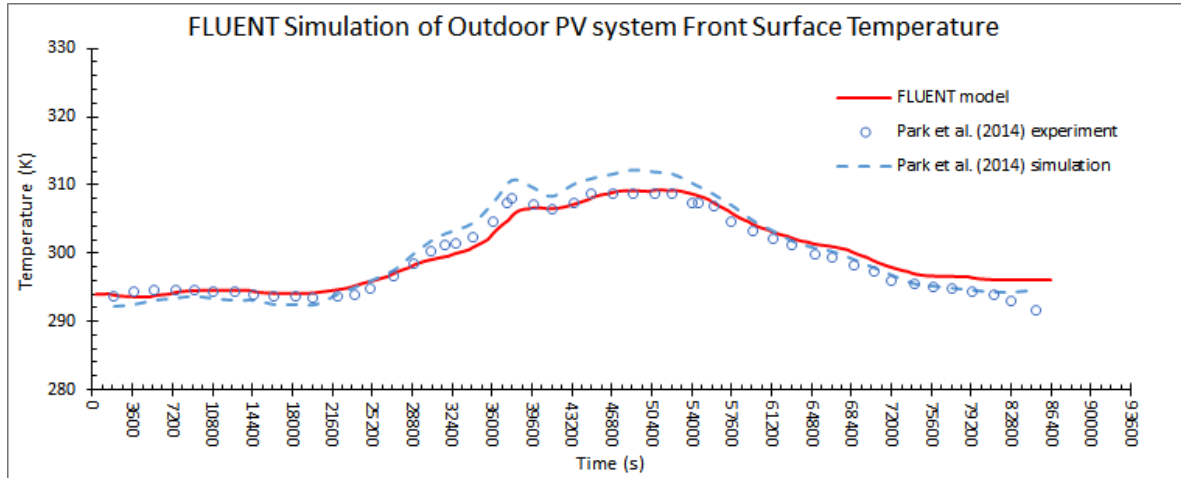
3. Outdoor PV Module

Figure 4.7: front surface temperature of the 3-D model of the outdoor PV module simulated in "FLUENT"

Figure 4.7 above shows an overall better proximity of the front surface temperature of the 3-D model of the outdoor PV module that was simulated by "FLUENT" to the experimental temperature distribution delivered by Park et al (2014) when compared to the temperature profile simulated by these authors. The maximum difference between the "FLUENT" simulation and experimental results does not exceed 4.6 K and occurs at the end of the simulation.
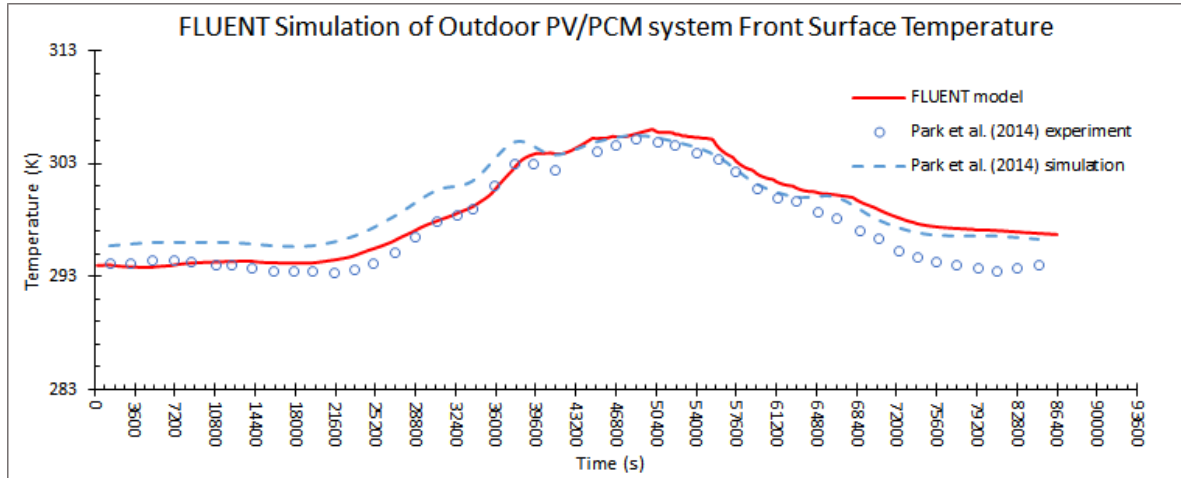
4. *Outdoor PV/PCM Module*

Figure 4.8: front surface temperature of the 3-D model of the outdoor PV/PCM module simulated in "FLUENT"

The "FLUENT" simulation and experimental temperature profiles of the front surface of the 3-D model of the outdoor PV/PCM module exhibit a close match as depicted in Figure 4.8 as the maximum difference between the two does not exceed 3.2 K.

C. OPENFOAM

For every model in "OpenFOAM", the probe function was utilized to record the temperature at multiple locations at the front surface of the system. Each case had its own specified writing interval. The recorded values were averaged to obtain a temperature distribution for the front surface of the system with time which was compared with the corresponding experimental data from Hasan et al. (2010) and Park et al. (2014).
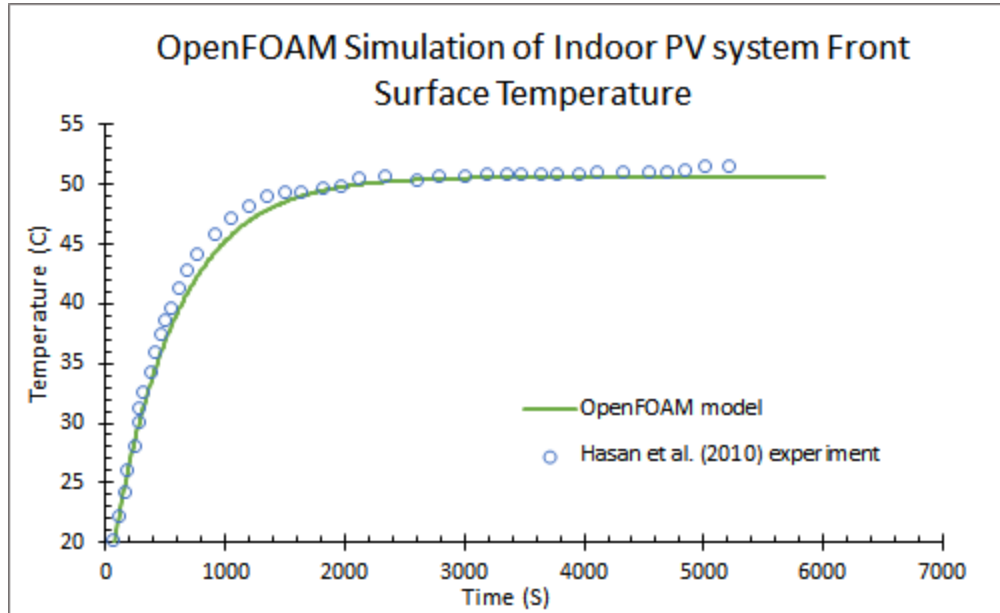
1. Indoor PV Module

Figure 4.9: front surface temperature of the 3-D model of the indoor PV module simulated in "OpenFOAM"

A close match can be noticed in Figure 4.9 above between the 3-D "OpenFOAM" model front surface temperature of the indoor PV module and the corresponding experimental temperature distribution from Hasan et al. (2010).
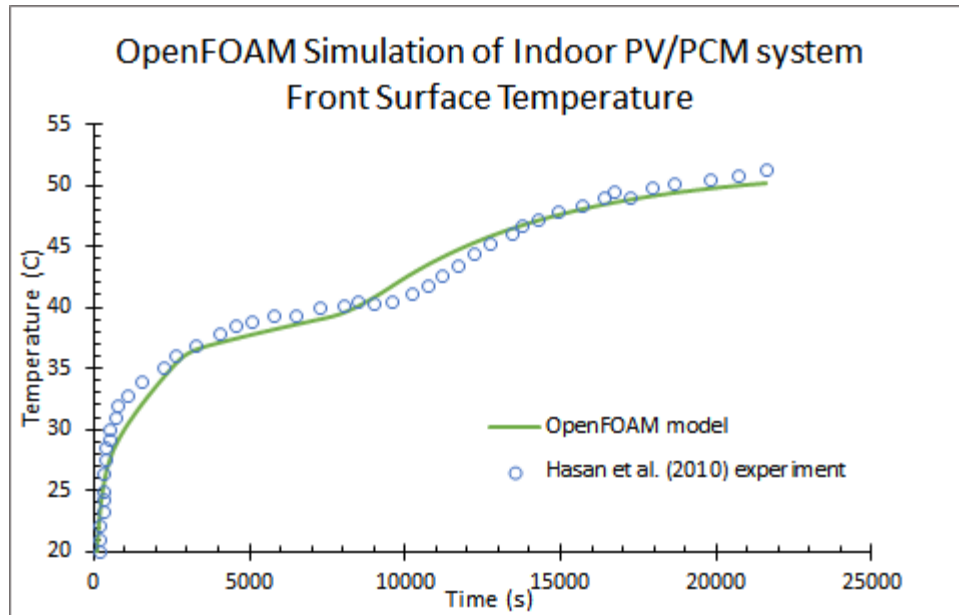
2. *Indoor PV/PCM Module*

Figure 4.10: front surface temperature of the 3-D model of the indoor PV/PCM module simulated in "OpenFOAM"

The 3-D "OpenFOAM" model of the indoor PV/PCM module resulted in an overall good agreement regarding the front surface temperature of the system when compared with the experimental data provided by Hasan et al. (2010) as shown in Figure 4.10 above; the maximum discrepancy was about 2.5 ℃ and occurred at the beginning of the simulation.

3. *Outdoor PV Module*
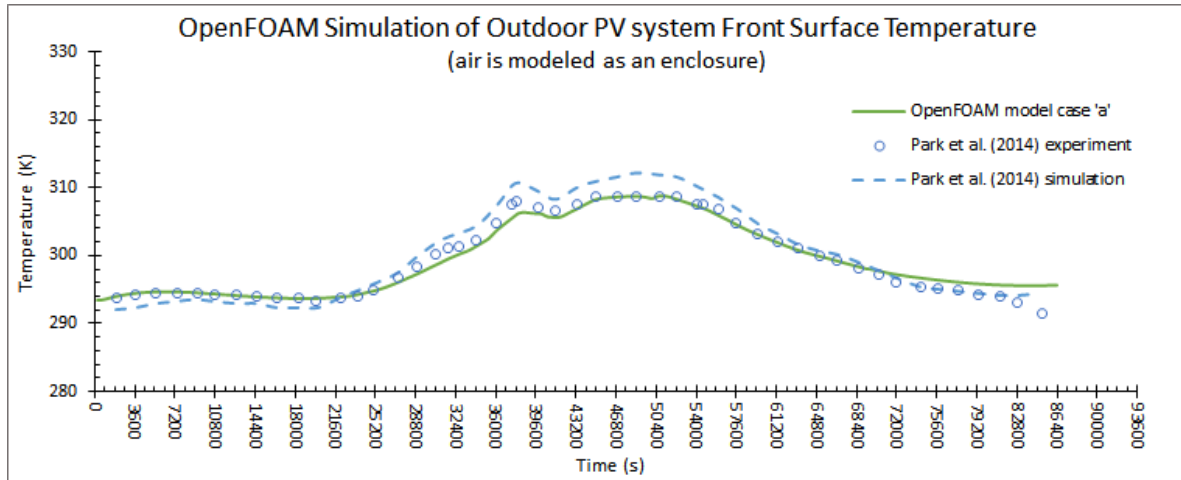
a. Outdoor PV module case 'a'

Figure 4.11: front surface temperature of the 3-D model of the outdoor PV module simulated in "OpenFOAM" case 'a'

As depicted in Figure 4.11, when air in the vicinity of the 3-D outdoor PV module is modeled in "OpenFOAM", the predicted front surface temperature was very close to the measured temperature profile of Park et al. (2014); the maximum discrepancy between the two profiles is about 4.1 K and can be noticed at the end of the simulation. Also, the temperature distribution attained with "OpenFOAM" model shows a better overall proximity to the experimental result as compared to the temperature profile obtained numerically by Park et al. (2014).
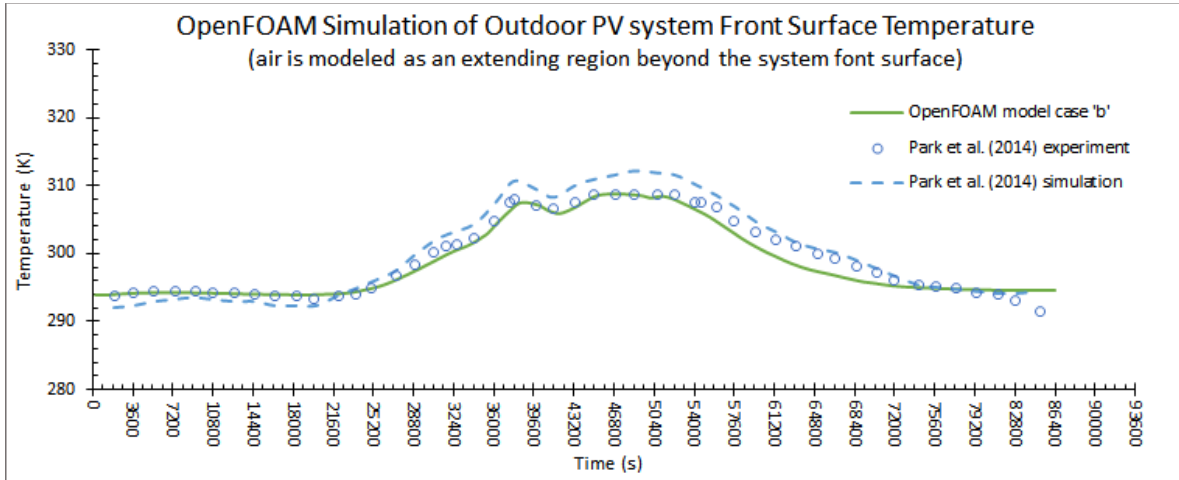
b. Outdoor PV module case 'b'

Figure 4.12: front surface temperature of the 3-D model of the outdoor PV module simulated in "OpenFOAM" case 'b'

After including the air region in contact with the front surface in the 3-D "OpenFOAM" model of the outdoor PV module, the temperature profile of the system's front surface obtained numerically by "OpenFOAM" exhibits a better proximity to the experimental data when compared with the corresponding simulation conducted by Park et al. (2014) as shown in Figure 4.12. A maximum difference of 3 K can be observed at the end of the simulation between the temperature profile experimentally recorded by Park et al. (2014) and that obtained from "OpenFOAM" model.

4. *Outdoor PV/PCM Module*

a. Outdoor PV/PCM module case 'a'

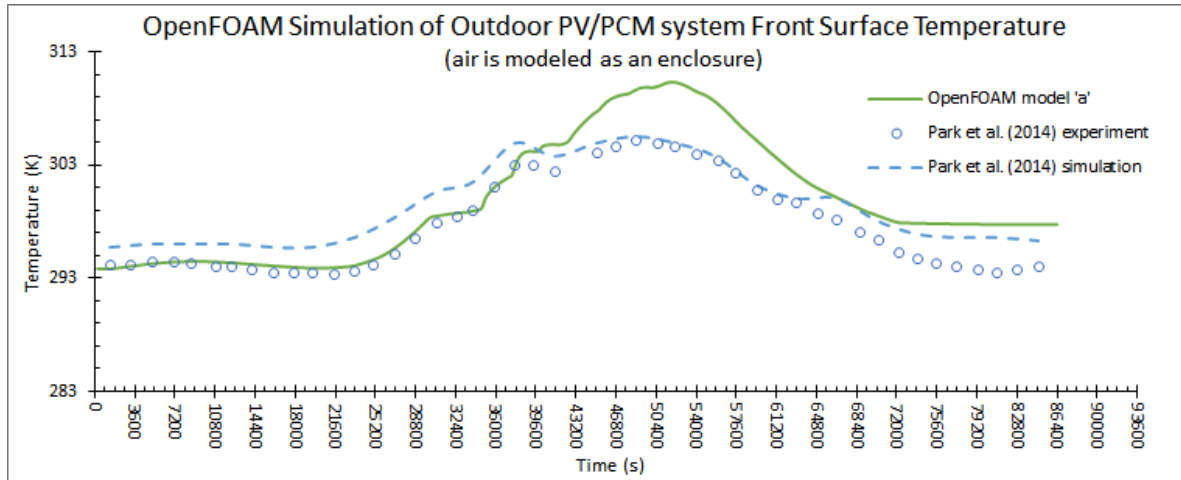Figure 4.13: front surface temperature of the 3-D model of the outdoor PV/PCM module simulated in "OpenFOAM" case 'a'

Figure 4.13 above depicts a large maximum discrepancy of 5.7 K between the front surface temperature distribution which was attained by modeling the outdoor PV/PCM module in "OpenFOAM" inside an air enclosure and the corresponding experimental front surface temperature profile.
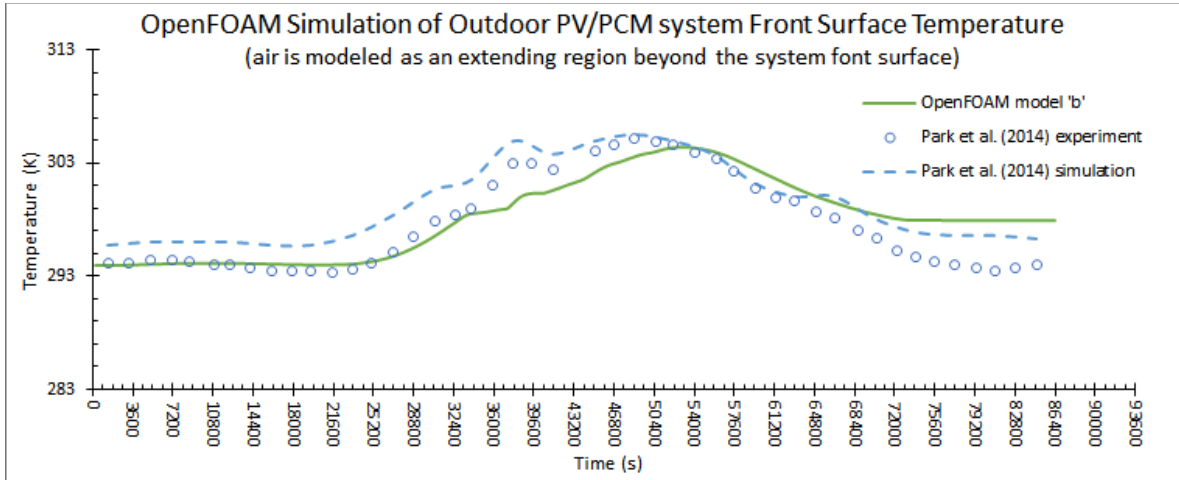
b. Outdoor PV/PCM module case 'b'

Figure 4.14: front surface temperature of the 3-D model of the outdoor PV/PCM module simulated in "OpenFOAM" case 'b'

When including the air region in contact with the front surface of the outdoor PV/PCM module in the 3-D "OpenFOAM" model, the numerically predicted temperature profile is shown in Figure 4.14 to be close to the corresponding experimental temperature profile although a time shift of about 4500 s could be observed between the peaks of the two profiles. The maximum difference between these two temperature distribution curves did not exceed 4.5 K and occurred towards the end of the simulation. Also, at some time steps especially at the beginning of the simulation, the temperature distribution that was attained via "OpenFOAM" exhibited a closer proximity to the experimental temperature profile than the temperature distribution resulting from the simulation that was carried by Park et al. (2014).

CHAPTER V

PARAMETRIC STUDY

The 3-D validated models of the indoor and outdoor modules are used in this chapter to conduct a parametric study to predict the variation in the module front surface temperature upon modifying some parameters.

A. INDOOR PV MODULE

The external radiation flux (750 W/m^2) used in the validated 3-D "OpenFOAM" model of the indoor PV module was replaced sequentially by a lower value of 500 W/m^2 and a higher value of 1000 W/m^2 in two separate parametric cases. The temperature distributions of the model's front surface for the two parametric cases compared to the base case are shown in Figure 5.1. The front surface temperature of the indoor PV module increases by 10 ℃ at steady state as the external radiation flux increases by an amount of 250 W/m^2.
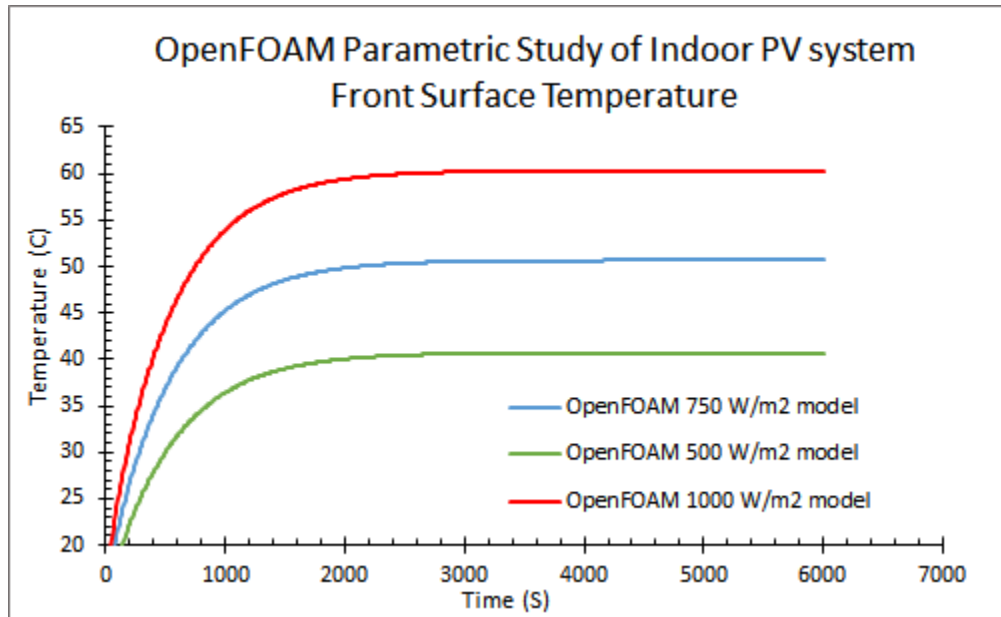
Figure 5.1: Indoor PV module front surface temperature of the 3-D "OpenFOAM" base model and corresponding parametric cases.

B. INDOOR PV/PCM MODULE

The phase change material employed in the validated 3-D "OpenFOAM" model of the indoor PV/PCM module was paraffin wax (RT 20) which has a solidus temperature Ts and liquidus temperature Tl values of 294.38 K and 298.88 K respectively (i.e. it has an average melting temperature $Tm = 296.63\ K$). Two parametric cases containing different types of PCM were simulated in "OpenFOAM" based on the validated model. While acetic acid which has a melting temperature lower than that of paraffin wax was used as the PCM in the first parametric case, the second case included capric acid that has a melting temperature higher than that of paraffin wax. Acetic acid and capric acid are non-paraffin organic PCMs that belong to the fatty acids group. The thermo-physical properties of

paraffin wax, acetic acid, and capric acid that are defined in the "transportProperties" and

"thermophysicalProperties" dictionary files are listed in Table 5.1.

Table 5.1: Thermo-physical properties of the PCMs used in the parametric study for the 3-D "OpenFOAM" model of the indoor PV/PCM module

	Paraffin Wax RT20	Acetic acid	Capric acid
"thermophysicalProperties" dictionary			
Number of moles	1	1	1
Molar weight (g/mol)	352	60.05	172.268[b]
Thermal Conductivity (W/m.K)	_	_	_
Dynamic Viscosity (Kg/m.s)	0.205	0.00131[a]	0.0043
Prandtl number	2152.5	14.5	46.28
Specific Heat Capacity (J/Kg.K)	2100	2000[a]	2760.76
Density (Kg/m^3)	825	1132[a]	893[b]
"transportProperties" dictionary			
Solidus Temperature (K)	294.38	289.85[a]	304.65[b]
Liquidus Temperature (K)	298.88	289.85[a]	304.65[b]
Latent Heat (J/Kg)	140300	187000[a]	153000

Table references: (a- Thermal-Fluids Central), (b- https://pubchem.ncbi.nlm.nih.gov/).

Figure 5.2 depicts the front surface temperature obtained from simulating the indoor

PV/PCM module in "OpenFOAM" using the three different PCMs. When a PCM with a

lower melting temperature such as acetic acid is used, the phase change starts earlier

compared to the base case with paraffin wax. On the other hand, the mushy zone is shifted

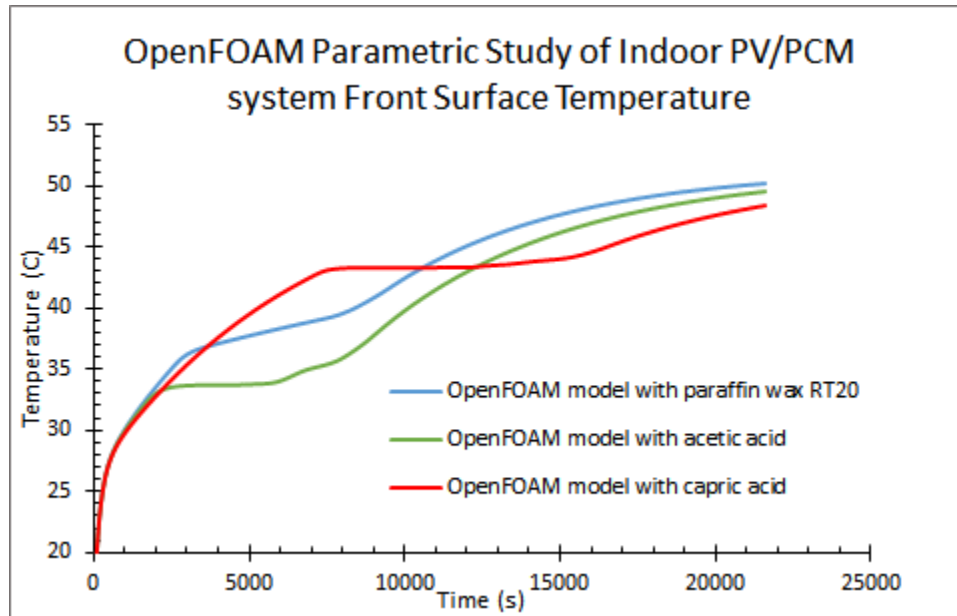forward in time upon replacing paraffin wax by a PCM with higher melting temperature such as capric acid.

Figure 5.2: Indoor PV/PCM module front surface temperature of the 3-D "OpenFOAM" base model and corresponding parametric cases.

C. OUTDOOR PV MODULE

For the validated 3-D "OpenFOAM" model case 'b' of the outdoor PV module, the geographic location at which the model was simulated was changed from Incheon, South Korea which is characterized by a mild climate to Dubai, UAE that is known for its hot weather. In both cases, the direct normal radiation is computed based on "ASHRAE clear sky model"; consequently the "radiationModel" and its corresponding sub model that are defined in the "radiationProperties" file of the air region are set to "solarLoad_amin1" and "solarCalculator_amin1" respectively. The historical weather data for Dubai on 15 June

2012 was extracted from "wunderground.com". An air velocity in the north direction with a magnitude of 12.73 Km/h (3.54 m/s) was obtained resulting in a velocity vector (3.54, 0, 0) m/s. Using this velocity, a heat transfer coefficient value of 8.456 W/m^{2}K was computed based on Ito (1972) model in the same way shown in chapter III. Also, the ambient air temperature distribution was extracted across 24 hours and it was implemented in the boundary conditions along with the air velocity and heat transfer coefficient in the same manner as in the base case. The "localStandardMeridian", "longitude", and "latitude" fields of the "radiationProperties" file of the air region were changed to 4, 55.17, and 25.07 respectively to account for the location change in the parametric case. A maximum increase of about 6 ºC in the temperature distribution of the parametric case front surface can be observed in Figure 5.3 below when compared to the corresponding temperature distribution of the base case.
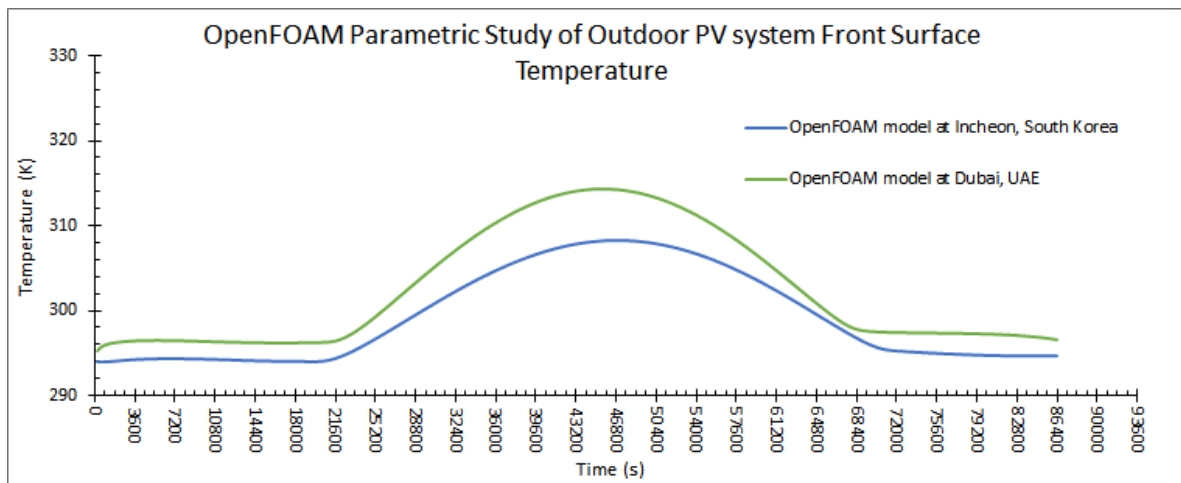

Figure 5.3: Outdoor PV module front surface temperature of the 3-D "OpenFOAM" base model and corresponding parametric case.

D. OUTDOOR PV/PCM MODULE

Similarly, the geographic location was altered from Incheon to Dubai to study the effect of replacing the mild weather by a hot one on the validated 3-D "FLUENT" model of the outdoor PV/PCM module. "FLUENT" "Solar Calculator" which uses "ASHRAE clear sky model" was assigned to compute the two "Solar Load Illumination Parameters", "Direct Solar Irradiation", and "Diffuse Solar Irradiation" for both cases. The same ambient air temperature distribution, air velocity, and heat transfer coefficient that were obtained for the previous parametric case of the outdoor PV module were used in this parametric case. Also, these quantities were employed in the boundary conditions in the same way as in the outdoor PV/PCM module base case. Furthermore, the fields "Longitude", "Latitude", and "Timezone" in the "Solar Calculator" were modified in the parametric case to 55.17, 25.07, and 4 respectively. As depicted in Figure 5.4, the PV/PCM module front surface temperature in the parametric case undergoes a maximum increase of about 21 ℃ in comparison with the corresponding temperature profile of the base case.
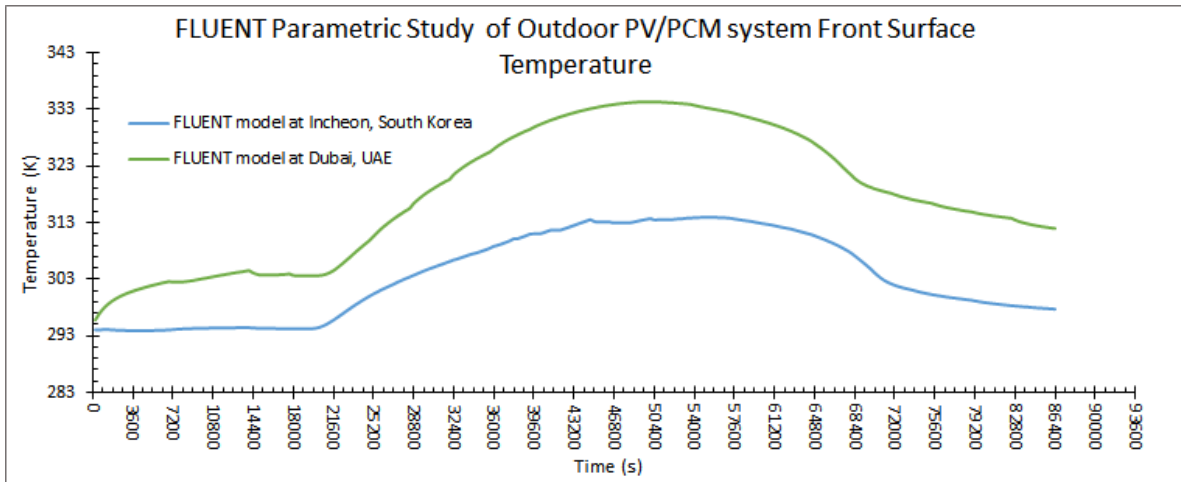
Figure 5.4: Outdoor PV/PCM module front surface temperature of the 3-D "FLUENT" base model and corresponding parametric case.

CHAPTER VI

CLOSURE

After simulating the indoor and outdoor PV and PV/PCM modules in 1-D and 3-D models, it turned out that the 1-D models generated the poorest results with respect to the experimental data. Moreover, both the open source CFD framework "OpenFOAM" and the commercial package "FLUENT" proved to be reliable tools for modeling the physical phenomena of radiation, solidification/melting, and solar radiation. Although "OpenFOAM" rivaled "FLUENT" in the considered cases, it can be noticed that the performance of "OpenFOAM" surpassed "FLUENT" regarding modeling the melting of phase change materials that do not melt at a single temperature rather they change phase within a melting range (i.e. the difference between liquidus and solidus temperatures) such as paraffin wax (RT 20). Furthermore, "OpenFOAM" offered a wider capability for creating new physical models, solvers, and boundary conditions besides modifying the existing ones compared to "FLUENT" through the direct implementation of C++ syntax code; it also showed a greater flexibility in adjusting the different terms of the governing equations for the various regions of the models.

The parametric study presented in chapter V included only a sample of the parameters that can be considered. For future work, it can be extended to include several other significant parameters such as investigating the effect of employing different thicknesses of the PCM layer, using other PCM types especially inorganic ones, modifying the dimensions and material of the enclosure containing the PCM such as using insulation

materials, and exploring other climatic conditions under which the models of the outdoor modules are simulated. In addition, the models of the PV/PCM modules can be further developed to include a solar thermal system to produce domestic hot water from the heat released by the PCM. Also, these models can be extended by adding wall layers to become models of building integrated PV/PCM modules to target the reduction of the cooling load in buildings besides improving the efficiency of PV panels.

REFERENCES

- ANSYS, Inc. 2011. ANSYS FLUENT Theory Guide 14.5. www.arc.vt.edu/ansys_help/flu_th/flu_th.html

- Armstrong, S., and W.G. Hurley. 2010. A thermal model for photovoltaic panels under varying atmospheric conditions. Applied Thermal Engineering 30: 1488-1495.

- Biwole, P.H., Eclache, P., and F. Kuznik. 2013. Phase-change materials to improve solar panel's performance. Energy and Buildings 62: 59–67.

- Ettouney, H., Alatiqi, I., Al-Sahali, M., and K. Al-Hajirie. 2006. Heat transfer enhancement in energy storage in spherical capsules filled with paraffin wax and metal beads. Energy Conversion and Management 47: 211–228.

- Hackbusch, W. 1985. Multi-Grid Methods and Applications. Berlin: Springer Inc.

- Hackbusch, W. 1994. Iterative Solution of Large Sparse Systems of Equations, New York: Springer-Verlag Inc.

- Hasan, A., McCormack, S.J., Huang, M.J., and B. Norton. 2010. Evaluation of phase change materials for thermal regulation enhancement of building integrated photovoltaics. Solar Energy 84: 1601-12.

- Hasan, A., McCormack, S.J., Huang, M.J., Sarwar, J., and B. Norton. 2015. Increased photovoltaic performance through temperature regulation by phase change materials: Materials comparison in different climates. Solar Energy 115: 264-76.

- Hendricks, J. H. C., and W. G. J. H. M. van Sark. 2013. Annual performance enhancement of building integrated photovoltaic modules by applying phase change materials. Progress in Photovoltaics: Research and Applications 21: 620-30.

- Ho, C.J., Tanuwijava, A.O., and C.M. Lai. 2012. Thermal and electrical performance of a BIPV integrated with a microencapsulated phase change material layer. Energy and Buildings 50: 331-8.

- Huang, M.J. 2011a. The effect of using two PCMs on the thermal regulation performance of BIPV systems. Solar Energy Materials and Solar Cells 95: 957-63.

- Huang, M.J., Eames, P.C., and B. Norton. 2004. Thermal regulation of building-integrated photovoltaics using phase change materials. International Journal of Heat and Mass Transfer 47: 2715-33.

- Huang, M.J., Eames, P.C., and B. Norton. 2006a. Phase change materials for limiting temperature rise in building integrated photovoltaics. Solar Energy 80: 1121-30.

- Huang, M.J., Eames, P.C., and B. Norton. 2006b. Comparison of a small-scale 3D PCM thermal control model with a validated 2D PCM thermal control model. Solar Energy Materials and Solar Cells 90: 1961-72.

- Huang, M.J., Eames, P.C., Norton, B., and N.J. Hewitt. 2011b. Natural convection in an internally finned phase change material heat sink for the thermal management of photovoltaics. Solar Energy Materials and Solar Cells 95: 1598-603.

- Krauter, S., and R. Hanitsch. 1996. Actual optical and thermal performance of PV-modules. Solar Energy Materials and Solar Cells 41-42: 557-74.

- Lamberg, P., and K. Sire´n. 2003. Analytical model for melting in a semi-infinite PCM storage with an internal fin. Heat and Mass Transfer 39: 167-76.

- Lamberg, P., Lehtiniemi, R., and A.M. Henell. 2004. Numerical and experimental investigation of melting and freezing processes in phase change material storage. International Journal of Thermal Sciences 43: 277-87.

- Lo Brano, V., Ciulla, G., Piacentino, A., and F. Cardona. 2013. On the Efficacy of PCM to Shave Peak Temperature of Crystalline Photovoltaic Panels: An FDM Model and Field Validation. Energies 6: 6188-210.

- Malvi, C.S., Dixon-Hardy, D.W., and R. Crook. 2011. Energy balance model of combined photovoltaic solar-thermal system incorporating phase change material. Solar Energy 85: 1440-46.

- Moukalled, F., Mangani, L., and M. Darwish. 2016. The finite volume method in computational fluid dynamics : an advanced introduction with OpenFOAM® and Matlab®. 1st ed 2015. Springer International Publishing Switzerland 2016.

- Murthy, J.Y., and S.R. Mathur. 2002. Numerical Methods in Heat, Mass, and Momentum Transfer. engineering.purdue.edu/ME608/webpage/main.pdf

- Park, J., Kim, T., and S.B. Leigh. 2014. Application of a phase-change material to improve the electrical performance of vertical-building-added photovoltaics considering the annual weather conditions. Solar Energy 105: 561-74.

- Radziemska, E., and E. Klugmann. 2002. Thermally affected parameters of the current–voltage characteristics of silicon photocell. Energy Conversion and Management 43: 1889-1900.

- Sharma, A., Tyagi, V.V., Chen, C.R., and D. Buddhi. 2009. Review on thermal energy storage with phase change materials and applications. Renewable and Sustainable Energy Reviews 13: 318-45.

- Twidell, J., and T. Weir. 2006. Renewable Energy Resources, 2nd ed. London: Taylor & Francis Group.

- Voller, V.R., Cross, M., and N.C. Markatos. 1987. An enthalpy method for convection/diffusion phase change. International Journal for Numerical Methods in Engineering 24: 271-84.

- Wilkes, K.E., Dinwiddie, R.B., and R.S. Graves. 1996. Thermal Conductivity 23. Technomic Publishing Company, Inc. U.S.A.